Combined control of bottom and turbidity currents on the origin and evolution of channel systems, examples from the Porcupine Seabight.

Verweirder, Lotte; Van Rooij, David; White, Martin; Van Landeghem, Katrien; Bossée, Kimberley; Georgiopoulou, Aggeliki

Marine Geology

DOI:
10.1016/j.margeo.2021.106639

Published: 01/12/2021

Peer reviewed version

Combined control of bottom and turbidity currents on the origin and evolution of channel systems, examples from the Porcupine Seabight.

L. Verweirder[a,*], D. Van Rooij[a], M. White[b], K. Van Landeghem[c], K. Bossée[a] & A. Georgiopoulou[d]

[a] Department of Geology, Ghent University, Krijgslaan 281 (S8), 9000 Ghent, Belgium

[b] Earth and Ocean Sciences, National University of Ireland, University Road, Galway, Ireland

[c] School of Ocean Sciences, Bangor University, Menai Bridge, Bangor LL59 5AB, UK

[d] School of Applied Sciences, University of Brighton, Cockcroft Building, Lewes Road, Brighton BN2 4GJ, UK

* Corresponding author. E-mail address: Lotte.Verweirder@UGent.be

Abstract

The Gollum Channel System (GCS) and Kings Channel System (KCS) are situated at a key location on the eastern side of the Porcupine Seabight to provide valuable insight into British-Irish Ice Sheet dynamics and sediment supply to the Belgica cold-water coral mound province. These channel systems are the most efficient pathways for particles from the Irish Shelf edge to the Porcupine basin. The spatial and temporal variability of their activity are, therefore, likely to have significant regional consequences. However, the sedimentary processes involved in the evolution of both systems have not yet been comprehensively studied. Here, bathymetric, 2D seismic reflection and oceanographic data are used to reconstruct and compare the interplay between along-, across- and downslope processes through geomorphologic and seismic stratigraphic analyses. The initial seafloor topography of the systems was shaped in the late Miocene-late Pliocene by intense northward-flowing bottom currents during the first phases of the composite RD1 erosion event. The bases of the KCS and GCS were eroded by downslope-flowing turbidity currents during the last phase of the RD1 event. Sediment transport within the channels was probably most active during Quaternary glacial periods of lowered sea levels, and sediment carried downslope by turbidity currents was likely pirated and transported northwards by contour currents. Therefore, the channels are proposed to have been of major importance as a source of sediment and nutrients for the Belgica cold-water coral mounds and associated sediment drifts to the north. The GCS and KCS represent an area where bottom currents, turbidity currents, slope failures and hemipelagic processes have interacted throughout the Neogene and Quaternary.

Keywords: Porcupine Seabight; submarine channel system; continental margin processes; seismic stratigraphy; sediment gravity flow; bottom current

1. INTRODUCTION

Submarine canyons are steep-walled features governed by erosional processes that are found incising shelves and slopes on continental margins across the world (Shepard, 1965; Harris and Whiteway, 2011; Harris et al., 2014). Canyons may transform basinwards into submarine channels (Babonneau et al., 2002; Deptuck et al., 2003; Cunningham et al., 2005) that are characterized by depositional components such as overbank levees, and have lower thalweg slope angles, a gentler topography and a generally more U-shaped cross-section compared to the upstream V-shaped canyons (Shepard, 1965; Weaver et al., 2000; Wynn et al., 2007; Amblas et al., 2018). These canyon-channel systems are major pathways for the transport of sediments and organic matter from the shelf and upper slope down to the abyssal plains (Shepard, 1965; Mulder, 2011; Puig et al., 2014). Given how important they have proven to be in, for example, regional sediment distribution (Amaro et al., 2016; Mountjoy et al., 2018; Maier et al., 2019) and hydrography (Xu and Noble, 2009; Hall et al., 2017; Waterhouse et al., 2017), it is important to understand how such large systems have behaved through time, especially long-lived canyon-channel systems.

The Gollum Channel System (GCS) on the Irish continental margin was first recognized on the bathymetric maps made by Brenot and Berthois (1962) and further described by Kenyon et al. (1978). In total, sixteen slope-confined to shelf-indenting tributary channels have now been distinguished on the upper eastern slope of the Porcupine Seabight (Fig. 1) (Kenyon et al., 1978; Beyer et al., 2007). The four northernmost channels were found to differ morphologically from the southern ones and were on that basis distinguished as a separate system known as the Kings Channel System (KCS; Fig. 1A) (Van Rooij, 2004; Beyer et al., 2007). Whereas the channels in the GCS join basinwards into one main channel leading to the Porcupine Abyssal Plain, the Kings channels terminate in an area on the slope that has a complex geomorphology and shows evidence of mass-wasting (Fig. 1C). At the distal end of the GCS, a deep-sea fan is present but only poorly developed (Rice et al., 1991; Akhmetzhanov et al., 2003), which is thought to be due to reworking of sediments by bottom currents (Rice et al., 1991).

Several sedimentary processes have been suggested as important components in shaping the KCS and GCS. The interplay between these processes, their variability through time, and their influence on channel evolution have not yet been comprehensively studied. They might, however, have significant regional consequences, as the GCS is the only major channel system in the Porcupine Seabight and therefore forms the most efficient pathway along which sediment and organic matter can be transported from the shelf downslope into the basin. This knowledge gap becomes especially obvious when comparing the GCS and KCS to canyon(-channel) systems on the Celtic and Armorican margins. Whittard Canyon, for example, has been investigated extensively with regard to the deglaciation history of the European Ice Sheet (Zaragosi et al., 2000; Bourillet et al., 2003; Toucanne et al., 2008), present-day canyon processes (Cunningham et al., 2005; Amaro et al., 2015; Carter et al., 2018; Daly et al., 2018), habitat suitability (Huvenne et al., 2011; Amaro et al., 2016), and hydrography (Wilson et al., 2015; Hall et al., 2017; Aslam et al., 2018). It has been proposed that during Quaternary glacial low-stands, the GCS formed the extension of a river system on the Irish Shelf (Kenyon et al., 1978; Weaver et al., 2000), although there is a lack of evidence to support this statement. Nevertheless, the proximity of sediment sources during glacial periods probably led to active downslope sediment transport within the system, i.e., mainly through turbiditic or other mass-wasting processes (Tudhope and Scoffin, 1995; Wheeler et al., 2003). Therefore, studying the variability in channel activity could provide insight into ice sheet dynamics during (the most recent) glacial period(s) (Toucanne et al., 2008). Furthermore, northerly contouritic currents infilling the channels have been inferred from geomorphology (Wheeler et al., 2003). Thus, the temporal variability in activity through the GCS and KCS is likely of high importance for sediment supply to the cold-water coral (CWC) mound provinces and contourite drifts that are found just north of the study area (Fig. 1A) (De Mol et al., 2002; Dorschel et al., 2007; Van Rooij et al., 2007a, 2009; Lim et al., 2018). Lastly, on the flanks of the channels in the GCS, broad terraces and numerous mass-wasting features such as slide and slump scars were recognized (Kenyon et al., 1978; Wheeler et al., 2003).

The aim of this study is, therefore, to characterize the sedimentary processes that affected the evolution of the KCS and GCS and more specifically the interplay between bottom and turbidity currents. The seabed morphology of four main channels (two in the KCS and two in the GCS; Fig. 1) and their surrounding slopes is first described. Subsequently, the subsurface sedimentary structures are linked to the existing chronostratigraphic framework and interpreted with regard to the processes that formed them, focussing on their role in regional sediment dynamics. Particular attention is paid to differences between the two channel systems, as well as between the channels of the eastern Porcupine Seabight and the Whittard Canyon on the Celtic Margin.

2. REGIONAL SETTING

2.1 GEOLOGICAL SETTING

The two channels in the KCS and two channel sections in the GCS studied here are situated on the eastern slope of the Porcupine Seabight, a pear-shaped oceanic basin located to the southwest of Ireland (Naylor and Shannon, 1982; Beyer et al., 2003). The basin is more than 3000 m deep in its deepest parts and is bounded by four shallower areas: Slyne Ridge to the north, the Irish Shelf to the east, Goban Spur to the south and the Porcupine Bank to the west. It has only a narrow opening towards the Atlantic Ocean in the southwest, therefore forming an embayment on the eastern North Atlantic continental margin (Fig. 1A). Underlying the Porcupine Seabight is the Porcupine Basin, which is a failed rift basin that formed from the Permian onwards (Shannon, 1991; Shannon et al., 2007). It experienced a major extensional period related to the opening of the North Atlantic in the Late Jurassic, followed by thermal subsidence from the Early Cretaceous to the Holocene (Shannon, 1991; McCann et al., 1995; Naylor and Shannon, 2005). The basin is now filled with up to 6 km of Mesozoic and up to 4 km of Cenozoic sediments (Moore and Shannon, 1992; Shannon et al., 2007).

Over the eastern side of the Porcupine Seabight, at least two major unconformities in the Cenozoic succession were recognized (Van Rooij et al., 2003) and sampled during Integrated Ocean Drilling Program Expedition 307 (IODP Exp. 307) (Expedition Scientists, 2005). The oldest unconformity, represented by the RD2 seismic reflector (Van Rooij et al., 2003), was attributed an early middle Miocene age (Louwye et al., 2008). It is roughly coeval to the erosional event represented by the C20 seismic reflector in the Rockall Trough and the Porcupine Basin (late early Miocene age) (McDonnell and Shannon, 2001; Stoker et al., 2001), and the two reflectors have been proposed to correspond, but have never been tied on any seismic line (McDonnell and Shannon, 2001; Van Rooij et al., 2003). Seismic data suggest that the C20 reflector is related to bottom current intensification, which was likely due to the introduction of Norwegian Sea Water into the North Atlantic (de Graciansky et al., 1984; McDonnell and Shannon, 2001; Stoker et al., 2005). The youngest unconformity, identified on seismic data as the RD1 reflector (Van Rooij et al., 2003), represents a large hiatus between upper Miocene and upper Pliocene sediments (Kano et al., 2007; Louwye et al., 2008). There is strong evidence that it is linked to the introduction of Mediterranean Outflow Water into the Porcupine area (Van Rooij et al., 2003; Khélifi et al., 2009; Delivet et al., 2016). It also marks the onset of Quaternary glacial-interglacial cycles and their influence on the oceanographic regime in the North Atlantic (McDonnell and Shannon, 2001; Van Rooij et al., 2003). Van Rooij et al. (2003) proposed that the RD1 discontinuity is equivalent to the intra-Pliocene C10 unconformity that is found across the NE Atlantic margin and thought to originate from tectonic uplift and deep-water erosion (Stoker et al., 2001, 2005). Based on the length of the RD1 hiatus at IODP Exp. 307 (late Miocene - late Pliocene), the C10 unconformity (intra-Pliocene) is enclosed within the RD1 unconformity (Stoker et al., 2001, 2005).

The main sediment sources for the eastern slope of the Porcupine Seabight are the broad Irish and Celtic shelves, and northwards flowing contour currents. The input from the Porcupine Bank is (and has been) likely much lower, which explains why only the eastern edge of the Seabight is characterized by channels (Rice et al., 1991). Numerous fine-grained turbidites have been found in cores in channel thalwegs and flanks downslope of the study area (Kenyon et al., 1998) and on the continental rise at the western end of the system (Akhmetzhanov et al., 2003). However, there are no indications of recent turbiditic transport through the channels, and both visual and core data suggest that downslope processes in the GCS have been inactive during the Holocene (Tudhope and Scoffin, 1995; Kenyon et al., 1998; Van Rooij et al., 2002; Akhmetzhanov et al., 2003; Wheeler et al., 2003). As the eastern slope of the Porcupine Seabight was situated 30-60 km from the ice limit of the British-Irish Ice Sheet (BIIS) during the Last Glacial Maximum (LGM) (Fig. 1A; Scourse et al., 2021), late Quaternary sedimentation is noticeably influenced by glacial activity. Ice-rafted debris, including dropstones, and increased sedimentation rates are related to the deglaciation of the area and retreat of the BIIS from the Irish Shelf after the LGM (Tudhope and Scoffin, 1995; Van Rooij et al., 2007a, 2007b). Reconstruction of the offshore extent of the BIIS before the LGM is problematic. Onshore, however, its lateral extent has been larger prior to the LGM, in particular during marine isotope stage 12 (MIS12) (Sejrup et al., 2005). Therefore, it could be expected that the offshore BIIS extent southwest of Ireland has been similar to the extent at the LGM, at least during MIS12. Finally, the importance of bottom currents for the depositional regime is demonstrated by the presence of contourite drifts associated with the CWC mounds of the Belgica Mound Province (BMP) (Van Rooij et al., 2003, 2007b, 2009), asymmetrical megaripples in the BMP (Lim et al., 2018), and asymmetrical cross-channel profiles in the GCS (Wheeler et al., 2003). In the upper section of one of the channels of the GCS, Tudhope and Scoffin (1995) reported ripples consisting of moderately well-sorted silty sands, and suggested they result from reversing currents within the channel.

2.2 OCEANOGRAPHIC SETTING

Within the Porcupine Seabight, bottom currents show a cyclonic flow pattern, flowing northwards along the eastern edge (White, 2007). Bottom residual currents flow on average towards 309°N, in a poleward and slightly off-slope direction, with a velocity of 2.5 cm/s (mooring 112 in Pingree and Le Cann (1990); location see Fig. 1B). The present-day water masses in the Seabight have been characterized as warm and saline Eastern North Atlantic Central Water (ENACW) in the upper 600 m, carried northward as part of the European Slope Current (ESC), and overlying Mediterranean Outflow Water (MOW) with a high-salinity core between 800 and 1000 m depth (Fig. 2) (Pingree and Le Cann, 1989; White, 2007; Toucanne et al., 2021). Additionally, low-salinity Labrador Sea Water (LSW) is present at about 1500-1900 m depth (Rice et al., 1991; Wienberg et al., 2020) and North East Atlantic Deep Water (NEADW) with influences of overflow waters from NE Atlantic basins below that (Rice et al., 1991; Van Aken, 2000). In particular, the long-term variation of the MOW has been a major influence on sedimentation in the Porcupine Seabight (Van Rooij et al., 2007a; White, 2007). At the permanent thermocline, which is situated at the depth of the boundary between the MOW and the overlying ENACW, freely propagating semi-diurnal or bottom-trapped diurnal internal tides (internal waves at tidal frequency) can be generated between 600 and 900 m water depth (Fig. 2) (Pingree and Le Cann, 1990; White, 2007; White and Dorschel, 2010). Both processes can enhance bottom current velocities, which may lead to resuspension and transport of sediments, thus affecting the slope morphology (White and Dorschel, 2010; Lamb, 2014).

3. MATERIAL AND METHODS

The study area comprises the upper slope section of the two main channels in the KCS and of the two northernmost channels of the GCS, which are the four channels that are covered by the multibeam bathymetry of Beyer et al. (2003) and by a grid of single-channel high-resolution seismic profiles (Fig. 1B). To better understand the local hydrography within a channel, data from a mooring within Bilbo Channel is added to the oceanographic information that is available from literature (Pingree and Le Cann, 1989; White, 2007).

3.1 MULTIBEAM BATHYMETRY

The bathymetry data used here are part of a larger dataset acquired during RV Polarstern cruise ANT XVII/4 in 2000 using a Hydrosweep DS-2 multibeam echosounder. The acquisition details are discussed in Beyer et al. (2003). The relevant section of the resulting DTM (with 50 m grid spacing) is here used without any additional processing (coloured area in Fig. 1B).

In the bathymetry analysis, the channel lengths are measured along the channel thalwegs defined in Fig. 1B. Channel width, channel depth and channel floor width are measured perpendicular to the thalweg and are the distances between, respectively, the two channel shoulders, the shallowest of the two shoulders and the thalweg, and the two points at the base of the channel where the slope angle changes abruptly (Fig. 3).

3.2 SINGLE-CHANNEL SEISMIC PROFILING

The single-channel seismic reflection profiles (Fig. 1B) were collected during five campaigns in 1999 (Belgica 99/13), 2001 (Belgica 01/12), 2003 (Belgica 03/13), 2006 (Belgica 2006/13) and 2018 (Belgica 2018/14). They were all obtained with RV Belgica, using an SIG sparker source and a single-channel SIG streamer. The main characteristics of each survey are summarized in Table 1. The profiles have a vertical resolution of about 1.5 m and the penetration depth is about 400 ms two-way travel time (TWT). The raw data were processed in RadExPro 2016.3 using an Ormsby bandpass filter, amplitude correction and a swell filter, where the settings for each filter were tailored for each profile. For some of the 1999 profiles, an F-K filter was applied as well. After processing, IHS Kingdom Suite software was used to plot and visualize the seismic profiles and trace the reflectors.

3.3 OCEANOGRAPHIC DATA

The mooring in Bilbo Channel sat underwater at a depth of 900 m for a period of 325 days, between June 2005 (Julian day 166) and May 2006 (Julian Day 126). It was located on the floor of the channel (Fig. 1B) and had one current meter at 8 m above the seafloor providing a measurement every 30 minutes. Due to biofouling, the current data is accurate only until December 2005. Therefore, current data from mid-December (Julian day 351) until the end of the measuring period is omitted from the analyses.

To estimate how internal waves interact with the seabed in the study area, the ratio of the slope angle γ to the angle of the internal wave energy propagation *c* is calculated over one slope transect (see Fig. 1A for location). Here, γ is calculated from bathymetry data, taking the slope correction into account (after Ribó et al. (2016)), while *c* is determined from the following formula (Cacchione et al., 2002):

$$c = \sqrt{\frac{\sigma^2 - f^2}{N^2 - \sigma^2}}$$

Herein, the internal wave frequency σ (expressed in cycles per hour, cph) is dependent on the dominant tidal frequency, which is here determined from the Bilbo mooring current meter data. The Coriolis frequency *f* [cph] at latitude φ is given by $f = (\sin\varphi)/12$. The Brunt-Väisälä frequency *N* [cph] varies with water depth and is calculated from a World Ocean Database 18 (WOD18) CTD station in the study area (Boyer et al., 2018; see Fig. 1B for location) using Ocean Data View (Schlitzer, 2020). The obtained values for *N* are averaged into depth intervals of 10 m to reduce noise.

4. RESULTS

4.1 SEABED MORPHOLOGY

4.1.1 KINGS CHANNEL SYSTEM

The KCS is, except for two channel heads, completely covered by the multibeam bathymetry of Beyer et al. (2003) (Fig. 1B). The two largest channels of the system are Aragorn Channel in the north and Theoden

Channel in the south (Fig. 1C). Both channels are U-shaped in cross-section. Aragorn Channel is oriented roughly ENE-WSW, is about 13 km long, 4.7 to 6.3 km wide and on average 300 m deep, with the channel depth increasing from 220 m in the east to almost 400 m in the west. The channel floor has an average slope gradient of 2.6° and is about 2.3 km wide in the eastern part, widening to 4.5 km towards the west. In the centre of the channel, an elongated mounded feature of 3.8 km long and 1.2 km wide is elevated maximum 100 m above the adjacent channel floor and separates the channel into two flow paths (Fig. 1C). A second mounded feature of about 45 m high lying against the northern channel flank measures 3.2 km in length and 1 km in width. The northern channel wall, with slope values of about 10-16° and up to 22°, is a bit steeper than the southern flank, where the slope measures 7-14° and up to 22°.

Theoden Channel is also oriented ENE-WSW, is 23 km long, and widens first from 4 to almost 6 km, after which it narrows again to about 3 km. The channel floor has a relatively constant width of about 1.3 km and an average basinward-dipping slope of about 2.2°. The depth of Theoden Channel first increases westwards, from 120 to 520 m, and then decreases again to 200 m. The northern flank of the channel has typical slope angles of 7-13° and up to 17°. The southern flank is a bit steeper with angles of 10-17°. Inside the channel against the northern channel flank lies an elongated mound of sediment that is about 7.5 km long, maximum 1.5 km in width, and at its highest point a little under 200 m above the adjacent channel floor. The southern flank of Theoden Channel is characterized by a clearly visible slide scar of 11 km² (Fig. 1C). On the smooth slopes north of Aragorn Channel and north of Theoden Channel, respectively 17 and 28 pockmarks with a diameter of about 150 m can be identified (Fig. 1E). It is likely that these pockmark fields contain even more individual pockmarks, as the numbers reported here are limited by the artefacts and the resolution of the bathymetry map (50 m; Beyer et al., 2003).

The Denethor area (Fig. 1C) covers at least 150 km², although its western extension is difficult to distinguish as the area is not fully enclosed in the multibeam data of Beyer et al. (2003). It has a very chaotic bathymetry where many scarps of 40-100 m high divide the seafloor into several blocks, ridges, and terrace-like features. Many of these scarps seem to be continuations of the flanks of Aragorn and Theoden channels, as well as the smaller channels between them. The largest of the scarps, however, is oriented

NW-SE and perpendicular to the channel axes (Fig. 1C). At this scarp, the slope angle is 19-26° and the depth difference is about 100 m over a horizontal distance of 350-450 m.

The slope to the east of the large scarp, in between Theoden Channel and a smaller channel, dips 2-6° to the SSW and is mostly smooth, aside from the pockmark field and five straight to slightly sinuous seafloor undulations (Fig. 1C). These undulations are about 1-4.5 km long and run parallel to each other with a general N-S orientation (170-175°N), roughly following the contour lines. They have an average wavelength of 1240 m (range = 730-2020 m) and an average height of 50 m (range = 20-110 m).

4.1.2 GOLLUM CHANNEL SYSTEM

Within the sections of Bilbo and Frodo channels that are presented here (approximately between the 500 and 1500 m water depth contours; Fig. 1B), the axes of both channels are generally straight and oriented ENE-WSW. However, in both channel sections, there are two places where the orientation changes by almost 90° that seem to be lined up between the two channels (Fig. 1D). The walls of Bilbo Channel have an average slope of 14-24°, but in some places can be as steep as 30°. The channel flanks of Frodo Channel have a slope that varies mostly between 10 and 20°, but the steepest sections also have a slope angle of up to 30°. In both channels, the northern channel flank is slightly steeper than the southern flank. Both channels are U-shaped in cross-section and both channel floors slope towards the basin at an average angle of about 2.2°. The depth of Bilbo Channel decreases from about 450 m in the east to about 250 m in the west. Its width is constant at 3.5-4 km, while the width of the channel floor is about 1.5 km throughout. The depth of Frodo Channel also decreases westwards, from about 350 m to 200 m. The width of the channel varies between 3.7 km (in the east) and 2.0 km (in the west), while the channel floor width is more constant varying between 0.8 and 1.2 km. A multitude of slide scars are visible on the channel walls. North of Bilbo Channel, the slope features a long scarp that is about 12.5 km in length and parallel to the channel axis (Fig. 1D). The difference in water depth over the scarp from north to south is about 40 m over a horizontal distance of about 450 m. The slope angle of the scarp is a bit higher (6-8°) than the slope of the surrounding seafloor (3-5°).

4.2 SEISMIC STRATIGRAPHY

The nomenclature for the seismic units and erosional surfaces observed here was adopted from the common nomenclature used on the eastern slope of the Porcupine Seabight (Van Rooij et al., 2007b, 2009).

4.2.1 UNIT U3

The lowermost unit visible on the seismic profiles in the KCS consists of high-amplitude continuous reflections that are mostly (sub)parallel and dipping towards the basin (Figs. 4-6). The upper 50-100 ms TWT (40-80 m using a P-wave velocity of 1600 m/s; Expedition Scientists, 2005) of the unit is organized in a wavy configuration in several places throughout the KCS (Fig. 6). The top of unit U3 is truncated by a regional discontinuity called RD2 (Figs. 4-6). In the GCS, unit U3 is not visible on any of the profiles.

4.2.2 UNIT U2

The RD2 erosional unconformity is the base of unit U2, which is almost acoustically transparent in the northern part of the study area. Parallel, basinward-dipping reflections can be distinguished, but with a lower amplitude and spaced further apart than those of unit U3 (Figs. 4, 6). Towards the southern end of the study area, however, U2 has fewer transparent sections and the parallel reflections are spaced more closely together (Fig. 5). The upper boundary of unit U2 is another regional discontinuity called RD1 (Figs. 4-9). Unit U2 has a very variable thickness throughout the study area, with values on average around 300 ms TWT (240 m), but with a maximum of around 450 ms TWT (360 m) on the interfluves and disappearing completely in the channels. North of Bilbo Channel at the top of the unit, a package of U2 reflections is truncated by an internal U2 reflection (Fig. 8).

On the northern flank of Aragorn Channel, two local subunits can be distinguished between unit U2 and RD1 (Figs. 4, 6). They are confined by erosional surfaces and their seismic facies is different from unit U2 below. The lowermost of the two subunits is called SUa. It consists of reflections of varying amplitudes that have a wavy character upslope and a parallel, downslope-dipping character towards the foot of the slope (Fig. 6). The reflections are down- or onlapping onto the lower erosional bounding surface, which is a local discontinuity called LD1a. In NNW-SSE profiles, the reflections of SUa are dipping to the south with varying angles and prograding in the same direction (Fig. 4). In WSW-ENE profiles, the wavy reflections can be seen migrating upslope (Fig. 6). The top of SUa is truncated by either RD1 or another local erosional surface called LD1b. Above SUa, the second subunit SUb is even more laterally restricted (Figs. 4, 6). The reflections in this subunit are subparallel and dipping towards the basin more gently compared to those in SUa. At the bottom of SUb, reflections are on- or downlapping onto LD1b, while at the top they are truncated by RD1.

4.2.3 REGIONAL DISCONTINUITY RD1

The upper boundary of unit U2 is the laterally extensive RD1 erosional surface. It has an irregular topography on the interfluves in the KCS, truncating reflections of unit U2 below (Figs. 4-6). The steepest slopes of the RD1 reflector, however, can be found underneath the channel edges, where it creates 0.4 s TWT (300 m) deep and 2-5 km wide U-shaped incisions in the paleotopography (Figs. 4, 5). In those locations, unit U2 is completely eroded and sediments at the top of unit U3 may have been removed as well. On the slope north of Theoden Channel and on the interfluves of the GCS, the RD1 reflector is generally less erosional and overlies U2 conformably (Figs. 7-9). The steepest slopes in the paleotopography of RD1 in the GCS are again visible on the channel edges, where the RD1 reflector cuts 0.4 s TWT (300 m) into U2 sediments, creating narrow (0.4-3 km), V-shaped incisions underneath the present-day channels.

RD1 truncates the reflections of the two local subunits north of Aragorn Channel (SUa and SUb) and the local erosional surfaces that bound them (LD1a and LD1b; Figs. 4, 6). Although the lateral extent of LD1b is very limited, LD1a is more extensive and created a rugged topography, potentially limiting the downslope extent of U2 sediments north of Aragorn Channel (Fig. 6).

4.2.4 UNIT U1

Above the RD1 unconformity, the uppermost seismic unit is called unit U1. On the slopes in between the channels, it consists of parallel-layered, high-amplitude reflections (Figs. 6-9). The same unit also constitutes the channel fills and in that setting typically includes more chaotic and transparent sections (Figs. 4, 5, 7). U1 reflections generally drape the RD1 unconformity conformably, but they can also be found on- or downlapping, especially where the RD1 event created a steep topography (Figs. 4, 6, 7).

4.2.4.1 U1 CHARACTERISTICS ON INTER-CHANNEL SLOPES

On the slopes between the channels, U1 reflections usually dip towards the basin (to the west) in E-W profiles and are near-horizontal in N-S profiles, except in proximity to the channels. Near the channels of the KCS, reflections of unit U1 dip towards the channels, with a steeper dipping angle closer to the channel. Several reflections can be followed from the channel edges towards the axis (Fig. 4). Near the channels of the GCS, the U1 reflections are near-horizontal or dipping away from the channel and are truncated at the channel edge (Fig. 7). Local divergence of reflections towards the channel is visible on the northern edge of the channels, over distances of about 1-4 km away from the channels and about 25 km downslope of the channel head (Figs. 4, 5, 7).

The stratification within unit U1 is usually very distinct, parallel and continuous, although there are some exceptions. Firstly, at the very top of the unit on the slopes north of Aragorn Channel and north and south of Theoden Channel, the reflections are interrupted by short (sub)vertical successions of small diffraction hyperbolas (Figs. 4-6). Several of these successions join the pockmarks on the seabed. Secondly, on the southern flank of Theoden Channel, unit U1 includes several erosional events (Fig. 5). Lastly, on the slope just north of Bilbo Channel, a large discontinuity (Fig. 8) is situated underneath the scarp in the bathymetry parallel to Bilbo Channel (Fig. 1D). It is related to the truncation of a package of sediments at the top of unit U2 (Fig. 8).

On the northern channel flank of Aragorn Channel, U1 is relatively thin (100-150 ms TWT or 80-120 m) compared to the southern Aragorn Channel flank (300-400 ms TWT or 240-320 m) and surrounding Theoden Channel (200-400 ms TWT or 160-320 m). North of Bilbo Channel, the thickness of U1 decreases from 300 ms TWT (240 m) in the east to 200 ms TWT (160 m) in the west (Figs. 7, 8).

On the slope north of Theoden Channel, undulating reflections are present from the seafloor down to the penetration depth of the seismic signal (Fig. 9). They make up the complete U1 sequence and even reach beyond the RD1 reflector, which has a conformable character in these profiles, into unit U2. They are usually laterally continuous, although some onlapping of reflections from the upslope flank of one undulation onto the downslope flank of the next undulation is visible just above and just underneath RD1 (Fig. 9). Especially underneath RD1 and in the lowest 150 ms TWT of unit U1, the upslope flanks of the undulations are thicker than their downslope flanks, causing them to migrate in an upslope direction. The thickness of both flanks of each undulation becomes more equal in the more recent deposits, and the undulations transition into a more aggradational configuration (Fig. 9).

Unit U1 on the slope north of Theoden Channel is not only characterized by the undulating reflections, but also by the truncation of the uppermost 120 ms TWT (100 m) of reflections west of the undulations. This truncation is situated at the location of the largest scarp of the Denethor area (Fig. 1C), which corresponds to the headwall of a submarine landslide. Underneath the truncated package, the reflections continue to the west and run parallel to the steep slope (Fig. 9). West of the large scarp, at the base of the slope, most of the terrace-like features in the Denethor area have an internal structure that is well-stratified, with reflections that are (sub)parallel and somewhat wavy or (slightly) dipping downslope, although some chaotic or transparent intervals are present as well (Fig. 9). The continuity of the reflections from one terrace to another is interrupted by diffraction hyperbolas, which are linked to the scarps and incisions in the bathymetry that create a rugged seafloor.

4.2.4.2 U1 CHARACTERISTICS IN CHANNEL INFILL

In the channels of the KCS, part of the channel infill consists of reflections that are continuous from the channel fill to the channel flanks, where they drape the RD1 unconformity. In the GCS, on the other hand, U1 reflections are truncated at the channel edge and do not form part of the channel infill.

The channel infills in Aragorn and Theoden channels are about 250 ms TWT (200 m) and 200-300 ms TWT (160-240 m) thick, respectively. The infills consist mainly of subparallel layered, slightly undulating reflections, with chaotic and transparent sections in between (Figs. 4, 5). Underneath, the base of the channel consists of the typical wavy and/or parallel reflections of relatively high amplitude of unit U3. The mounded features in both channels contain mostly continuous, parallel, high-amplitude reflections that dip towards the basin and have a convex-up shape in an across-slope profile, while at their bases a transparent to incoherent facies is present (Figs. 4, 5).

In Bilbo and Frodo channels, the infills are about 200 ms TWT (160 m) and maximum 300 ms TWT (240 m) thick, respectively. A high-amplitude reflection presumably indicates the bases of the channels, though it is not always clearly defined on the seismic data. The channel infills are composed of a chaotic to transparent facies including a couple of discontinuous, high-amplitude reflections (Fig. 7).

4.3 HYDROGRAPHY

The time series in Fig. 10A shows that the daily mean current in the recorded period never exceeded 14 cm/s. The maximum instantaneous current velocity measured 53.7 cm/s, but the average measured current speed was 15.1 cm/s and 70% of the measurements were lower than 20 cm/s (Fig. 10B, D). The overall residual current in the channel from June to December 2005 at 8 m above the channel floor was oriented towards 324°N (≈ NW) with a velocity of 4.75 cm/s (Fig. 10C). Tidal analysis indicates that the M_2 component (principal lunar semidiurnal; 12.42 hour period) dominates. The major axis of the M_2 tidal ellipse has an amplitude of 17.1 cm/s and is oriented along 100-280°N. The minor axis has an amplitude of 0.01 cm/s, hence the M_2-tide is strongly rectilinear along the channel axis (Fig. 10C). The tidal ellipses of the S_2- and the K_1-tides are both oriented along the channel axis as well (100-280°N and 90-270°N, respectively). The ellipse of the S_2-tide (principal solar semi-diurnal; 12 hour period) has a major axis with an amplitude of 9.2 cm/s (minor axis: -0.2 cm/s), while the K_1 (lunar diurnal; 23.93 hour period) tidal ellipse has a major axis with an amplitude of 1.0 cm/s (minor axis: -0.2 cm/s). Spring-neap cycles are also clearly visible in the data (Fig. 10E).

As the mooring results indicate that M_2 is the dominant tide in the study area, the internal wave frequency σ is set to 0.081 cph in the calculation of the γ/c-ratio that is used to estimate the interaction of internal waves with the seabed (Cacchione et al., 2002). Results from this calculation indicate that principal critical conditions ($\gamma/c \approx 1$) occur between 600 and 800 m water depth and more sporadically between 1000 and 1200 m water depth (Fig. 11A). In waters shallower than 600 m, subcritical conditions ($\gamma/c < 1$) prevail, while between 800 and 1000 m water depth, supercritical conditions are dominant ($\gamma/c > 1$).

5. DISCUSSION

5.1 CHRONOSTRATIGRAPHIC FRAMEWORK

Connecting seismic lines (e.g., the profile shown in Fig. 4) allow the seismic stratigraphy in the KCS and GCS to be linked to the seismic stratigraphy established in the BMP and Enya CWC mound area (Van Rooij et al., 2007b, 2009). Units U1, U2 and U3, and regional discontinuities RD1 and RD2 described here are the southward continuations of units U1, U2 and U3, and regional discontinuities RD1 and RD2 (respectively) as described in Van Rooij et al. (2007b, 2009). Local discontinuity LD1a is equivalent to RD1b in Van Rooij et al. (2009). Unit U2bis of Van Rooij et al. (2009) in the area of the Enya CWC mounds is here divided into two local subunits SUa and SUb, as local discontinuity LD1b, not recognized before, exists between them. Van Rooij et al. (2007b, 2009) linked the seismic stratigraphy of the Belgica and Enya CWC mounds to the litho- and chronostratigraphy of (the slope surrounding) Challenger Mound. These were determined during IODP Exp. 307 and described by Expedition Scientists (2005), Kano et al. (2007) and Louwye et al. (2008), and are used here to build the chronostratigraphic framework for the upper slope of the KCS and GCS.

Unit U3 is the lowermost unit visible on the seismic profiles. It is present at the base of some of the channels (Fig. 5) and in the channel flanks (Fig. 4). The lower boundary of this unit is not visible on any of the seismic profiles in the study area but has been recognized (without age determination) in the BMP (Van Rooij et al., 2007a, 2007b). The sediments within unit U3 are thought to be of early to middle Miocene age (Van Rooij et al., 2003). The upper boundary of unit U3 is an unconformity created by the RD2 erosional event (Van Rooij et al., 2003), which caused a minor hiatus that was attributed an early middle Miocene age (Louwye et al., 2008).

Unit U2 is bounded at the base by the RD2 unconformity and at the top by the RD1 erosional unconformity, which represents a large hiatus between upper Miocene and upper Pliocene sediments (Kano et al., 2007; Louwye et al., 2008; Van Rooij et al., 2009). The youngest dated sediments in unit U2 were deposited 8.96 Ma (Kano et al., 2007). However, the RD1 event eroded the sediments of unit U2 with varying intensity (Kano et al., 2007; Louwye et al., 2008; Huvenne et al., 2009), which is also indicated by the lateral thickness variations in the unit (Figs. 4, 5). As a result, seismic unit U2 in the study area is thought to include sediments of middle to late Miocene age, although deposition might have continued longer as it is unknown how much sediment was removed during the RD1 event.

Van Rooij et al. (2009) found that the RD1 event was locally preceded by another phase of erosion and in the data presented here, an additional very local erosion surface is recognized. These three unconformities are only distinguished with confidence north of Aragorn Channel (Figs. 4, 6) and they are indicated as LD1a (oldest, local phase), LD1b (younger, very local phase), and RD1 (youngest, extensive main phase). The LD1a unconformity has been attributed to an early erosional phase within a composite event, possibly masked further south by the more severe RD1 phase (Van Rooij et al., 2009). The same reasoning can be applied to explain the formation of the LD1b unconformity. Units SUa, present between LD1a and LD1b/RD1, and SUb, present between LD1b and RD1, could then consist of the deposits of these early phases within the composite RD1 event (Van Rooij et al., 2009), and thus be between late Miocene and late Pliocene in age. It should be noted, however, that this interpretation was based on the position of LD1a within the seismic stratigraphy and on a composite event with a possible earlier onset creating a better chronological fit between RD1 and regional erosion events (Van Rooij et al., 2009). These erosion surfaces might, therefore, not have any geological relation to the RD1 event, and simply be independent local events.

Sedimentation resumed asynchronously after the RD1 event, thus adding to the lateral variation in the extent of the RD1 hiatus and causing a variation in the age of the base of unit U1. Deposition after RD1 started 2.7 Ma with the onset of CWC mound growth in the BMP (Kano et al., 2007; Huvenne et al., 2009; Thierens et al., 2013). The CWC framework allowed baffling of sediments probably from around 2.6 Ma (Foubert and Henriet, 2009; Thierens et al., 2010). In locations where no CWC framework was present to promote the entrapment of grains, currents were periodically strong enough to winnow any sediments deposited during periods of weaker current regimes (Huvenne et al., 2009; Mienis et al., 2009; Thierens et al., 2010). This is exemplified in an off-mound site of IODP Exp. 307, where prolonged sedimentation after the RD1 event did not resume before 1.7 Ma (Kano et al., 2007; Huvenne et al., 2009). As the youngest dated sediments underneath RD1 were assigned an age of 8.96 Ma, the length of the RD1 hiatus based on IODP Exp. 307 data is 6-7 Myr (Kano et al., 2007; Huvenne et al., 2009; Thierens et al., 2010). Unit U1 in the study area is therefore suggested to consist of sediments of middle Early Pleistocene and younger ages.

5.2 EVOLUTION AND REGIONAL IMPORTANCE OF THE KINGS AND GOLLUM CHANNEL SYSTEMS

5.2.1 EARLY AND MIDDLE MIOCENE: PRE-CHANNEL SLOPE SEDIMENTATION

Seismic unit U3 mainly consists of siltstone (Expedition Scientists, 2005). Its seismic signature of predominantly subparallel, downslope dipping (3.5-4.5°) reflectors represents relatively calm paleoceanographic conditions with hemipelagic sedimentation during the early Miocene (Van Rooij et al., 2003; Louwye et al., 2008). The wavy reflectors that are present locally (Fig. 6), however, might represent sediment waves, which would be indicative of the presence of increased bottom currents (Van Rooij et al., 2003; Wynn and Masson, 2008). These structures have also been observed within U3 in upslope areas in the BMP (Van Rooij et al., 2003, 2007a), demonstrating that these more dynamic conditions in the early Miocene were more widespread than they might seem from the data shown here.

Seismic unit U2 is more acoustically transparent than unit U3, but also contains continuous reflections that are gently dipping towards the basin and are spaced more closely towards the southern end of the study area. IODP Exp. 307 data show that the sediments within U2 are mostly homogenous silty clays, especially at the bottom of the unit, though the clays are more interbedded with clayey silts and fine sands towards the top of the unit (Expedition Scientists, 2005). These factors point towards another period where hemipelagic sedimentation was the dominant process of deposition. Unit U2 also contains sediment waves north of Theoden Channel that are the subsurface expression of the undulations visible on the present-day seafloor (Fig. 9).

5.2.2 LATE MIOCENE – LATE PLIOCENE: INCIPIENT CHANNEL SYSTEMS

From similar seismic signatures of unit U2 north and south of individual channels (especially Aragorn and Bilbo channels; Figs. 4, 7), it is clear that the bases of the KCS and GCS are cut into the sediments of unit U2, which were originally deposited more uniformly across the margin. Additionally, some reflectors within U1 are continuous from the channel flanks to the channel axis (Figs. 4, 5), suggesting they were deposited across the slope after the initial incision of the channels. In the KCS, the RD1 event appears to have completely eroded unit U2 at the location of the channel bases, and may have partially eroded unit U3 (Figs. 4, 5). From these findings, it seems plausible that the extensive late Miocene-late Pliocene RD1 erosional event was responsible for initially shaping the KCS. It is likely that the RD1 event also provided the initial seafloor topography on which the GCS was built, as U2 reflections are truncated at the channel edges. However, the channel bases of the two northernmost channels of the GCS are situated at greater depths than those of the KCS, making it more difficult to determine the exact relation between the channels and the RD1 event from the seismic profiles (Fig. 7). Seismic profiles with deeper penetration are needed to clarify this relationship.

It has been proposed that the RD1 event was a composite event consisting of at least two separate phases (Van Rooij et al., 2009). The data presented here suggest that RD1 is the composite of at least three erosional phases that alternated with periods where local deposition of sediments was possible. Those depositional periods are represented by units SUa and SUb, which both show similarities with highly energetic contourite drift deposits (Stow et al., 2002; Van Rooij et al., 2009); the complex seismic signature with sigmoidal to wavy reflectors of unit SUa indicates a much more dynamic sedimentary environment during their deposition than for the sediments in unit U2 underneath. Within unit SUb, reflections are dipping more gently and are not as wavy as in SUa, but they do display onlap relationships with the LD1b unconformity, suggesting a relatively calmer though still current-influenced depositional environment. This illustrates the clear influence of bottom currents of varying intensities on shaping the initial seafloor topography where the channels developed. It also confirms the presence of high-energy northerly bottom currents in the late Miocene-late Pliocene period as suggested by Van Rooij et al. (2003) in the BMP. In contrast to the RD1 erosional event in the BMP, however, which is caused by bottom current action only (Van Rooij et al., 2003), the RD1 erosion in the study area is due to the combined effect of intensified bottom currents interrupted or followed by downslope flows finally creating the bases of the KCS and GCS. These erosive downslope flows originate from the Irish Shelf, where lowered sea levels in glacial periods generate more proximal sediment sources (Kenyon et al., 1978; Weaver et al., 2000). This accentuates the link between the RD1 event and the onset of glacial-interglacial cycles in the North Atlantic (Van Rooij et al., 2003). It also confirms that these channel systems could contain valuable information on BIIS dynamics at its southwestern limit, though further research will be needed to validate this and extract this information.

5.2.3 PLEISTOCENE – RECENT: CHANNEL INFILL AND FLANK BUILD-UP

5.2.3.1 TURBIDITY CURRENTS WITH SPATIALLY AND TEMPORALLY VARYING INTENSITIES

The importance of turbidity currents in shaping the channels is demonstrated by multiple fine-grained turbidites found in cores in channel thalwegs and flanks (Kenyon et al., 1998), as well as on the continental rise at the western end of the system (Akhmetzhanov et al., 2003).

In the KCS, several indications exist for turbidity currents changing in intensity throughout the Quaternary. Distinct discontinuities within unit U1 on the flanks of Theoden Channel point to periods of erosion causing repositioning or reshaping (broadening) of the channel alternating with periods of deposition causing channel infilling (Fig. 5). Furthermore, the three mounds of sediment within Aragorn and Theoden channels (Figs. 1C, 4, 5) are interpreted as internal levees (*sensu* Callow et al., 2014) based on their elongated shape parallel to the channel axis, their location within the channel, and the (sub)parallel, downslope-dipping seismic reflectors they are built from. The presence of internal levees suggests that the Kings channels evolved in such a way that they became capable of accommodating downslope flows. Larger channel dimensions were possibly combined with weaker and thinner flows resulting in the deposition of layered sediments in internal rather than on external levees (Deptuck et al., 2003; Callow et al., 2014). At the base of Theoden Channel, another set of layered reflections possibly hints at the presence of a buried internal levee (Fig. 5). It could indicate that, although erosional processes were dominant in the very beginning of KCS development creating their U-shaped bases, depositional processes took over soon after. Additionally, it could indicate lateral migration of the channel thalweg, although additional seismic data, and data reaching deeper into the subsurface, are needed to confirm this.

After the initial predominantly erosional to bypassing turbidity current action in the GCS, evidenced by V-shaped cross-sections, turbidity currents became bypassing to slightly depositional and started to fill the channels, creating more U-shaped cross-sections. In the lower section of unit U1 on the channel flanks, divergence of reflectors and a consequential increase in thickness of the unit towards the channels indicate the build-up of levees in very close (1 km) proximity to the channels (Figs. 7, 8). This suggests that turbiditic spillover played a role in shaping the channel flanks. However, the limited extent of the levees both northwards and westwards indicates that spilling was minimal (Mulder, 2011) and concentrated in the upslope section of the channel. The levee geometry diminishes towards the top of unit U1, where sediments are mostly draped onto the already existing topography, with reflections that are conformable, laterally continuous and have very limited thickness variations over large distances (Figs. 7, 8). This suggests a subsequent dominance of hemipelagic processes in the area , which is in accordance with hemipelagic muds devoid of turbidites found in cores on the flank of Frodo Channel (Kenyon et al., 1998). These observations indicate that the sediment load of any turbidity current flowing through the channels more recently than the levee deposition was completely confined within the channel (Weaver et al., 2000). This could be due to either higher channel flanks relative to the thickness of the flow, very infrequent occurrence of turbidity currents, an insufficient amount of suspended sediment within them, or a combination of these (Babonneau et al., 2002; Deptuck et al., 2003, 2007). The transition from a system dominated by turbidity currents to one where hemipelagic sedimentation prevails could be linked to a disconnection from the sediment source and accordingly a diminished sediment supply from the shelf during interglacials (Mulder, 2011). The combination of depositional (levees) and erosional characteristics (steep flanks with numerous slope failure scars; Fig. 1D), as well as the transition from V- to U-shaped cross-sections, allows for interpreting this upper slope section of the GCS as a canyon-channel transition (Kenyon et al., 1978; Mulder, 2011; Puig et al., 2014).

Whereas the KCS has been dominated by depositional processes interrupted by some erosional events, the turbidity currents in the Frodo and Bilbo channels in the GCS seem to have been predominantly erosional, with some deposition in outer levees (Figs. 4, 5, 7). In the GCS, channel fills are dominated by transparent facies typical for mass-transport deposits with sparse and discontinuous higher-amplitude reflections deposited from coarse-grained turbidity currents (Deptuck et al., 2003; Mulder, 2011). This is in contrast to the channel fills in the KCS, which are dominated by a facies with continuous, subparallel and sometimes undulating reflections deposited from more fine-grained flows running through the channels, intercalated with the transparent facies from mass-transport deposits (Figs. 4, 5). Generally, a more depositional environment is linked to slower currents allowing suspended sediments to settle, while the more erosional environment in the GCS might suggest overall more intense currents that inhibit deposition (Babonneau et al., 2002; Mulder, 2011). Intense currents combined with the strongly incised morphology of the GCS likely prevented large spillover, which may have led to a preservation of the energy of the turbidity currents, allowing them to continue all the way to the abyssal plain. In the KCS, on the other hand, more deposition from currents may have caused more energy loss and currents only reaching the base of the upper slope. This process has been used by Babonneau et al. (2002) to explain morphological differences between the Zaire and Amazon canyon-channel systems. As there is no significant difference in thalweg slope gradient between the two channel systems (about 2° in both systems), the difference in downslope current intensity inferred here must be explained otherwise. The channels of the KCS seem to be oriented towards the southwestern tip of Ireland (Fig. 1A), possibly indicating more direct access to terrestrial sediments, while the GCS channels are not oriented towards Ireland and may have been fed by material from the Irish Shelf. This possibly led to a difference in the amount and/or nature of sediment supplied to both systems. The higher current intensity and longer extent of the GCS seem to imply a higher sediment load in this system, though the existence of dilute flows causing significant erosion and little channel infill has been suggested as well (Babonneau et al., 2002). If the former hypothesis is true and large amounts of sediment were carried to the abyssal plain, currents there must have been strong enough to either reroute sediment elsewhere, or rework the sediments after deposition, and prevent a significant deep-sea fan from developing. The uncertainty about the nature and amount of sediment supply from the BIIS to the channel systems forces this reasoning to remain speculative.

5.2.3.2 SIGNIFICANCE OF BOTTOM CURRENTS IN A TURBIDITY CURRENT-DOMINATED SYSTEM

Although mass-wasting and turbiditic deposits dominate the channel fills and the lower part of unit U1 on the channel flanks in close proximity to the channel axes, and hemipelagic deposits dominate the rest of the areas in between the channels, several sections of unit U1 are clearly influenced by bottom currents. One such area can be found buried north of Aragorn Channel (Fig. 6). Another is the area of seafloor and connected subsurface undulations north of Theoden Channel (Fig. 9). Gravity processes deforming sediments are one of the mechanisms capable of shaping the seafloor into a “wavy” morphology (Faugères et al., 2002; Lee et al., 2002). However, in the study area, the seismic data show no evidence for sediment deformation in or near the undulating features, which are therefore interpreted as a sediment wave field formed by bottom currents. These sediment waves indicate the movement of sediment over this slope area during the late Miocene and throughout the Quaternary. As they are visible on the seabed (and thus not buried by hemipelagic sedimentation), whichever process is responsible for their build-up has likely been active until recently (Faugères et al., 2002).

Several mechanisms are known to form sediment waves: (1) deposition from along-slope flowing bottom currents (Masson et al., 2002; McCave, 2017), (2) deposition from downslope flowing turbidity currents (Migeon et al., 2000; Normark et al., 2002), or (3) deposition from across-slope oscillating internal waves (Ribó et al., 2016; Collart et al., 2018; Mestdagh et al., 2020). A combination of these processes has been suggested as well (Faugères et al., 2002). The orientation of the wave crests roughly perpendicular to the channel axes and parallel to the isobaths (170-175°N; Fig. 1C) precludes an origin from along-slope currents or turbiditic spillover. Sediment waves formed by sheet-like unconfined turbidity currents usually display a trend of decreasing dimensions downslope, are often linked to upslope slump and/or debris flow deposits, and are thought to require regular flow of turbidity currents over the area (Wynn et al., 2000; Ercilla et al., 2002; Kolla et al., 2021). Neither downslope decreasing dimensions nor associated gravity flow deposits are visible here (Fig. 9). Additionally, turbidity currents in the study area are thought to have been too intermittent (i.e., glacial-interglacial variability; Kenyon et al., 1998; Akhmetzhanov et al., 2003) to have formed such regular and vertically extensive sediment waves. However, the contribution of unconfined turbidity currents to the formation of the sediment wave field cannot be excluded completely and requires further research.

The sediment waves occur on the seafloor at 500-800 m water depth (Fig. 1C), a range which includes the interface between the ENACW and the underlying MOW (600-800; Fig. 2) and is roughly the depth of the permanent thermocline (600-900 m; White and Dorschel (2010)). The permanent thermocline is associated with increased baroclinic (internal) energy at tidal periods because of strong vertical density stratification there (Pomar et al., 2012; Shanmugam, 2013). Both semi-diurnal (freely propagating) and diurnal (bottom-trapped) baroclinic waves occur and enhance bottom turbulence (White and Dorschel, 2010; Pomar et al., 2012; Shanmugam, 2013), making both types plausible factors in the sediment wave generation.

The sediment waves are present where an area with little evidence of diurnal waves (at mooring 112; Fig. 1B) transitions to an area with strong diurnal waves (BMP). In the BMP, the resulting strong diurnal bottom currents were likely crucial for coral mound growth (White, 2007; White and Dorschel, 2010; Wienberg et al., 2020). Some modest enhancement of the diurnal tide might be expected in the study area, hence potentially the sediment waves might result from a localised region of bottom-trapped wave enhancement dependent on stratification, bottom slope and orientation of the barotropic diurnal tide.

Internal tides of semi-diurnal period will freely propagate within a stratified fluid at latitudes < ~75° (Morozov and Pisarev, 2002). At the ENACW-MOW interface (≈ permanent thermocline here), freely propagating internal tides have been predicted for a large part of the eastern slope of the Porcupine Seabight (Rice et al., 1990; White, 2007). The interaction of internal waves with a continental slope differs depending on the ratio of the seafloor slope angle γ to the incidence angle of the internal wave characteristics c: the waves are reflected upslope (transmissive conditions) when the slope is subcritical ($\gamma/c < 1$), reflected downslope (reflective conditions) when the slope is supercritical ($\gamma/c > 1$), or reflected parallel to the bottom when the slopes match ($\gamma/c \approx 1$) (Cacchione et al., 2002). In the latter case of a critical slope, the vertical wavelength approaches zero and the wave energy density is significantly enhanced (Lamb, 2014). This leads to increased bottom current velocities and shear stress, which may cause resuspension and transport of sediments, and induce the formation of sediment waves (Cacchione et al., 2002; Lamb, 2014; Ribó et al., 2016). Calculations of the γ/c-ratio using CTD data close to the sediment wave field (Fig. 1B) indicate that criticality conditions for the dominant M_2-tide occur within the depth range where the sediment waves are present, near the present-day permanent thermocline between 600 and 800 m (Fig. 11).

Given the proximity of the mooring 112 location (Pingree and LeCannn, 1990), freely propagating internal waves along the ENACW-MOW interface rather than bottom-trapped baroclinic diurnal tides are suggested as the most probable mechanism for the generation of the sediment waves on the seafloor north of Theoden Channel. Current measurements in the sediment wave field would help validate this hypothesis. Additionally, further research with deeper seismic data is needed to explain the occurrence of the sediment waves underneath RD1 (before the MOW existed; Hernández-Molina et al., 2014). Prior to MOW presence, a permanent thermocline would still have been present, so it is possible that internal waves existed in the depth range of the present-day ENACW-MOW boundary. Furthermore, there is evidence for a vertical shift of the permanent thermocline region over time (Raddatz et al., 2014; Wienberg et al., 2020), hence a deeper thermocline depth (with enhanced baroclinic energy) would be possible prior to MOW presence. A lack of knowledge on the paleoceanography in the study area before the RD1 event hinders verifying this possibility.

In seismic unit U2 and the lower part of unit U1, a slight offset of reflectors between two adjacent sediment waves points to erosional conditions on the downslope flanks in the period before and just after the RD1 event (Symons et al., 2016). Towards the top of unit U1, the reflectors become laterally continuous (and thus completely depositional) and the configuration of the sediment waves evolves from strongly upslope migrational into more aggradational (Fig. 9). This suggests a lessened influence of bottom current activity , possibly combined with relatively lower sedimentation rates (Flood, 1988; Wynn and Masson, 2008; Faugères and Mulder, 2011).

A third area that has likely been influenced by bottom currents is the Denethor area, though further research is needed to better understand its formational history. The parallel-layered reflections that are dominant in the internal structure of the individual terrace-like features (Fig. 9) indicate a possible combined influence of downslope-flowing turbidity currents and along-slope flowing bottom currents. Sediment brought into the basin by turbidity currents was likely subjected to pirating by northwards flowing contour currents towards the BMP along the steep slope-parallel escarpment in the Denethor area and the along-slope channel just north of the KCS (Fig. 1B) (Van Rooij et al., 2003). Thus, as they were the conduits for sediment transfer from the Irish Shelf to the Porcupine basin, the channels played an important role in the development of the Belgica CWC mounds and the associated sediment drifts.

Lastly, the slight asymmetry of the Gollum channels (with steeper northern flanks) may be linked to the action of northward-flowing bottom currents. The northern channel flanks create an obstacle for the currents, which causes intensification and erosion, whereas the southern flanks are predominantly areas of deposition (Figs. 7, 8; Marchès et al., 2007; De Mol et al., 2011).

5.2.3.3 SLOPE FAILURES AND THEIR ORIGIN

Apart from down-, across- and along-slope currents, the channels in the KCS and GCS are also shaped by numerous slope failure events (Figs. 1C, 1D). Undercutting of the channel walls by erosional downslope flows has been suggested as a major cause of slope failures in this setting (Micallef et al., 2012; Watson et al., 2020). Additionally, the presence of pockmark fields in the KCS (Fig. 1E) indicates the possible importance of excess pore pressure in the sediments for slope destabilisation (King and MacLean, 1970; Hovland and Judd, 1988; Hovland et al., 2002; Judd and Hovland, 2009), especially for the slope failures on the southern flank of Theoden Channel and at the southeastern edge of the Denethor area (Fig. 1C). The build-up of excess pore pressure might be linked to elevated sedimentation rates (Judd and Hovland, 2009; Moernaut et al., 2017), which are known to have occurred in the study area in the early period of deglaciation after the LGM (Van Rooij et al., 2007a, 2007b). The long scarp north of Bilbo is linked to a large discontinuity of the reflectors in the subsurface where a package of reflectors is truncated (Fig. 8), and is therefore suggested to be the seabed expression of a buried landslide headwall.

5.3 PRESENT-DAY IN-CHANNEL OCEANOGRAPHIC PROCESSES: TIDAL FORCING AND TURBIDITY CURRENT ACTION

The presence of the sediment wave field north of Theoden Channel and the general morphology of the study area, including smoothened channel flanks and smooth interfluves (Figs. 1B, 4, 5, 7), demonstrate the present-day influence of bottom currents on seafloor morphology between the channels (Wheeler et al., 2003; White, 2007). Inside the channels, Tudhope and Scoffin (1995) inferred reversing currents from channel floor ripples and estimated current velocities of 0.5 m/s. Measurements from the mooring in Bilbo Channel indicate a dominance of tidal forcing on the currents (Fig. 10E) up to a maximum of ~0.5 m/s comparable to the estimates of Tudhope and Scoffin (1995). Currents are dominated by the M_2-tide, strongly steered along the channel axis (Fig. 10C) and spring-neap as well as longer period cycles clearly visible in instantaneous current measurements (Figs. 10B, E). The currents measured inside the channel are more intense than those on the interfluve between the KCS and GCS (mooring 112; Fig. 1B) (Pingree and Le Cann, 1990; White, 2007), further demonstrating the significant influence of the topographically steered tidal motions in the channel. The overall residual current vector (Fig. 10C) and the daily mean current vectors (Fig. 10A) suggest the presence of a cross-channel component in the currents. This may be due to highly localized steering from an irregular channel floor topography, although this cannot be confirmed as the mooring is situated just outside the area covered by Beyer et al. (2003) bathymetry and detailed channel floor morphology is not available.

The instantaneous current measurements of the Bilbo mooring show no major (downslope) flow episodes and the mooring remained in the same position during the measurement period. This suggests that no major turbidity currents occurred in Bilbo Channel during that time and reinforces the idea that the channels are currently inactive with respect to sediment gravity flows. However, the possibility remains that turbidity currents occur too infrequently to have been detected by this mooring.

5.4 COMPARISON WITH WHITTARD CANYON ON THE CELTIC MARGIN

Whittard Canyon is the most westerly of the canyon systems on the northern continental slope of the Bay of Biscay (Fig. 1A). As the GCS, Whittard Canyon is a dendritic system that has been affected by turbidity current activity (Toucanne et al., 2008), and experiences some influence from tides causing present-day up-canyon sediment transport (Amaro et al., 2015) and from contour currents smoothening canyon flanks (Stewart et al., 2014). Canyon incision in the Whittard system started in the Pliocene-Pleistocene and is linked to lowered sea levels (Bourillet et al., 2003), similar to what is inferred here for the GCS. As the drainage system of the Grande Sole drainage basin, Whittard Canyon is thought to have drained the Celtic Sea during the last glacial period, receiving sediment from the BIIS (through the Irish Sea Ice Stream; Fig. 1A) and feeding the Celtic Deep-Sea Fan (Scourse et al., 2000, 2009; Zaragosi et al., 2000, 2006; Toucanne et al., 2008). The deglaciation of the most recent British-Irish and European ice sheets (ca. 20-13 ka), in particular, caused increased sediment influx to the Grande Sole drainage basin and consequently enhanced turbidity current activity in Whittard Canyon (Zaragosi et al., 2000; Bourillet et al., 2003; Toucanne et al., 2008). Terrigenous sediment input from glacio-isostatic uplift of the British Isles continued until 7 ka

(Lambeck, 1996; Bourillet et al., 2003). Even though Whittard Canyon is now too far from any coastlines and hemipelagic sedimentation influenced by tides and waves dominates the Celtic Margin, sediment gravity flows reworking material on the outer shelf and possibly induced by storm depressions or anthropogenic activity are still active within the Whittard system, although less frequently than during the last deglaciation (Zaragosi et al., 2000; Bourillet et al., 2003; Cunningham et al., 2005; Amaro et al., 2015; Daly et al., 2018).

Even though the Quaternary activity within Whittard Canyon seemingly bears many similarities to the GCS, the geomorphology of the two systems differs. Whittard Canyon is much more like a canyon system *sensu* Shepard (1965) consisting of an extensive dendritic network of conduits with steep walls (commonly 30-40°) incised by numerous gullies, clearly V-shaped cross-sections and large relief, that are in some places cutting into bedrock (Cunningham et al., 2005; Stewart et al., 2014). The present-day V-shaped cross-sections indicate that Whittard Canyon has been governed by erosional processes (Cunningham et al., 2005) more so and until more recently than the GCS. This might be due to the large amounts of sediment that were brought to the Whittard Canyon from the BIIS (Toucanne et al., 2008). As yet, there is uncertainty about 1) the extent of the BIIS before the LGM on the shelf southwest of Ireland and thus the efficiency of the (repeated?) connection to the GCS and KCS (Sejrup et al., 2005), and 2) the proportion of sediment sourced from the BIIS that reached the eastern slope of the Porcupine Seabight compared to the Celtic Margin. Therefore, it remains difficult to assess the influence of a potential difference in the amount of supplied sediment in the two systems. The absence of turbidity current activity in the GCS in the last 10 kyr (Wheeler et al., 2003) is probably due to a lack of sediment supply and/or external forces driving downslope flow (Mulder et al., 2012; Amaro et al., 2015). This is, however, not likely to be the most significant driver for the geomorphologic difference between the two systems, although very recent activity in Whittard Canyon does flush the canyons, depositing sediments further down the slope rather than in the channel axes (Amaro et al., 2015).

Another factor that might play a role is the difference in the average angle of the continental slope between the two areas: 2-5° on the eastern slope of the Porcupine Seabight versus an average of 8° on the

Celtic Margin (Piper and Normark, 2009; Mulder et al., 2012). A higher slope gradient could explain the higher dendricity in the Whittard Canyon system (Harris and Whiteway, 2011), and could also lead to a higher velocity and therefore more erosional character of turbidity currents flowing through the system (Piper and Normark, 2009; Mulder, 2011).

The presence of fault scarps at the seafloor suggests a significant and active tectonic control on the morphology of the Whittard system (Cunningham et al., 2005). In the GCS, geological control on the orientation and morphology of the channels has been hypothesized (Wheeler et al., 2003). Lined-up features such as sudden, sharp (90°) changes in otherwise straight channels (Bilbo and Frodo; Fig. 1D) could be an argument for that hypothesis, but it should be tested with deeper seismic data.

6. CONCLUSIONS

The first detailed seismic stratigraphy over the Kings and Gollum Channel Systems on the eastern side of the Porcupine Seabight is presented here. It is used to shed light on the processes involved in the evolution of the two systems, with a focus on their temporal variability, the interplay between them and their importance for regional sediment dynamics.

- The early to late Miocene pre-channel sedimentation is mainly hemipelagic, deposited in calm oceanographic conditions that were interrupted by a period with increased bottom current influence in the late early or early middle Miocene. In the early middle Miocene, erosion caused a small hiatus in the upper slope sedimentation. The margin-wide deposited pre-channel sediments were eroded during the extensive late Miocene-late Pliocene RD1 erosional event.
- The RD1 event is here proposed to have consisted of at least three phases of erosion. The first two phases are only recognized locally and resulted from highly energetic bottom currents that subsequently deposited the eroded sediments as high-energy drift deposits, shaping the initial seafloor topography where the channels developed. The youngest phase in the RD1 event was the most extensive, and, whereas it is attributed to intense bottom currents in the BMP, it is here associated with erosive downslope flows creating broader U-shaped incisions in the KCS and narrower V-shaped incisions in the GCS.

- The RD1 event has been linked to the onset of Quaternary glacial-interglacial cycles in the North Atlantic, and to the introduction of MOW into the NE Atlantic (Van Rooij et al., 2003). The combined effect of both processes (i.e., erosive downslope flows and intensified bottom currents) is visible in the multi-phased characteristics of the event in the KCS and GCS. This indicates that these channel systems could contain valuable information on BIIS dynamics at its southwestern limit, but further research will need to confirm this.
- Quaternary sedimentation is notably influenced by both bottom and turbidity current activity. There are strong indications that internal tides are present at the ENACW-MOW interface in at least part of the study area. They are suggested to have occurred throughout the Quaternary, with a diminishing intensity towards the present day. Turbidity currents were most active in the beginning of the channel evolution. They were more erosional in the GCS, while the KCS has been a predominantly depositional environment. They likely varied in intensity through time but eventually, a disconnection from sediment sources led to a dominance of hemipelagic sedimentation. There are no signs of recent turbidity current activity through the channels. The timing of the sediment source disconnection is uncertain. The upper slope sections of the KCS and GCS are nowadays a predominantly depositional environment where sedimentation is dominated by hemipelagic processes influenced by bottom current activity.
- Sediment carried downslope by turbidity currents was likely pirated and transported northwards towards the BMP by contour currents along slope-parallel escarpments and channels. Therefore, it is here proposed that the channels were of major importance as a source of sediment for the Belgica CWC mounds and the associated sediment drifts.
- The morphological difference between the channels on the eastern slope of the Porcupine Seabight and the Whittard Canyon is likely largely due to a greater sediment supply towards the Celtic Margin during glacial periods combined with a greater slope gradient and possibly an underlying tectonic control.

ACKNOWLEDGEMENTS

L. Verweirder was supported through a doctoral scholarship of the Ghent University Special Research Fund (BOF) and is currently funded by the Research Foundation – Flanders (FWO grant 1114521N). The data used in this article were acquired within the framework of the EC MAST ENAM II (1996-1999), EC FP5 GEOMOUND (2000-2003) and EC FP6 HERMES (2005-2008) projects. Ship time on RV Belgica was provided by BELSPO and RBINS–OD Nature. The authors wish to thank the ship crews involved in collecting the data, and the two anonymous reviewers for their contribution in improving this manuscript. This research was performed in collaboration with the "Source-to-sink sedimentary processes in and from the Celtic Sea (SPICES)" research group.

DATA AVAILABILITY

The seismic reflection data from campaigns Belgica 99/13 [https://doi.org/10.1594/PANGAEA.451881], Belgica 01/12 [https://doi.org/10.1594/PANGAEA.451889] and Belgica 03/13 [https://doi.org/10.1594/PANGAEA.451884] can be found in the PANGAEA data repository. The bathymetry data can be found at https://doi.org/10.1594/PANGAEA.763062, also in the PANGAEA repository. Data from campaigns Belgica 2006/13 and Belgica 2018/14, as well as the data from the Bilbo mooring, are part of ongoing research and are not available in any repository yet.

REFERENCES

Akhmetzhanov, A., Kenyon, N.H., Ivanov, M., Cronin, B.T., 2003. The Continental Rise West of Porcupine Seabight, Northeast Atlantic, in: Mienert, J., Weaver, P. (Eds.), European Margin Sediment Dynamics: Side-Scan Sonar and Seismic Images. Springer Science & Business Media, pp. 187–192.

Amaro, T., de Stigter, H., Lavaleye, M., Duineveld, G., 2015. Organic matter enrichment in the Whittard Channel; its origin and possible effects on benthic megafauna. Deep. Res. Part I Oceanogr. Res. Pap. 102, 90–100. https://doi.org/10.1016/j.dsr.2015.04.014

Amaro, T., Huvenne, V.A.I.A.I., Allcock, A.L., Aslam, T., Davies, J.S., Danovaro, R., De Stigter, H.C., Duineveld, G.C.A.A., Gambi, C., Gooday, A.J., Gunton, L.M., Hall, R., Howell, K.L., Ingels, J., Kiriakoulakis, K., Kershaw, C.E., Lavaleye, M.S.S.S., Robert, K., Stewart, H., Van Rooij, D., White, M., Wilson, A.M., 2016. The Whittard Canyon – A case study of submarine canyon processes. Prog. Oceanogr. 146, 38–57. https://doi.org/10.1016/j.pocean.2016.06.003

Amblas, D., Ceramicola, S., Gerber, T.P., Canals, M., Chiocci, F.L., Dowdeswell, J.A., Harris, P.T., Huvenne, V.A.I., Lai, S.Y.J., Lastras, G., Lo Iacono, C., Micallef, A., Mountjoy, J.J., Paull, C.K., Puig, P., Sanchez-Vidal, A., 2018. Submarine Canyons and Gullies, in: Submarine Geomorphology. Springer, pp. 251–272.

Aslam, T., Hall, R.A., Dye, S.R., 2018. Internal tides in a dendritic submarine canyon. Prog. Oceanogr. 169, 20–32. https://doi.org/10.1016/j.pocean.2017.10.005

Babonneau, N., Savoye, B., Cremer, M., Klein, B., 2002. Morphology and architecture of the present canyon and channel system of the Zaire deep-sea fan. Mar. Pet. Geol. 19, 445–467. https://doi.org/10.1016/S0264-8172(02)00009-0

Beyer, A., Chakraborty, B., Schenke, H.W., 2007. Seafloor classification of the mound and channel provinces of the Porcupine Seabight: an application of the multibeam angular backscatter data. Int. J. Earth Sci. 96, 11–20. https://doi.org/10.1007/s00531-005-0022-1

Beyer, A., Schenke, H.W., Klenke, M., Niederjasper, F., 2003. High resolution bathymetry of the eastern slope of the Porcupine Seabight. Mar. Geol. 198, 27–54. https://doi.org/10.1016/S0025-3227(03)00093-8

Bourillet, J.F., Reynaud, J.-Y., Baltzer, A., Zaragosi, S., 2003. The “Fleuve Manche”: The submarine sedimentary features from the outer shelf to the deep-sea fans. J. Quat. Sci. 18, 261–282. https://doi.org/10.1002/jqs.757

Boyer, T.P., Baranova, O.K., Coleman, C., García, H.E., Grodsky, A., Locarnini, R.A., Mishonov, A. V., Paver, C.R., Reagan, J.R., Seidov, D., Smolyar, I. V., Weathers, K.W., Zweng, M.M., 2018. World Ocean Database 2018. A.V. Mishonov, Techincal Editor. NOAA Atlas NESDIS 87.

Brenot, R., Berthois, L., 1962. Bathymétrie du secteur atlantique du banc Porcupine (ouest de l’Irlande) au cap Finisterre (Espagne). Rev. des Trav. l’Institut des Pêches Marit. 26, 219–273. https://doi.org/10.1016/0011-7471(63)90388-7

Cacchione, D.A., Pratson, L.F., Ogston, A.S., 2002. The shaping of continental slopes by internal tides. Science (80-.). 296, 724–727. https://doi.org/10.1126/science.1069803

Callow, R.H.T., Kneller, B., Dykstra, M., McIlroy, D., 2014. Physical, biological, geochemical and sedimentological controls on the ichnology of submarine canyon and slope channel systems. Mar. Pet. Geol. 54, 144–166. https://doi.org/10.1016/j.marpetgeo.2014.02.016

Carter, G.D.O., Huvenne, V.A.I., Gales, J.A., Lo Iacono, C., Marsh, L., Ougier-Simonin, A., Robert, K., Wynn, R.B., 2018. Ongoing evolution of submarine canyon rockwalls; examples from the Whittard Canyon, Celtic Margin (NE Atlantic). Prog. Oceanogr. 169, 79–88.

https://doi.org/10.1016/j.pocean.2018.02.001

Collart, T., Verreydt, W., Hernández-Molina, F.J., Llave, E., León, R., Gómez-Ballesteros, M., Pons-Branchu, E., Stewart, H., Van Rooij, D., 2018. Sedimentary processes and cold-water coral mini-mounds at the Ferrol canyon head, NW Iberian margin. Prog. Oceanogr. 169, 48–65. https://doi.org/10.1016/j.pocean.2018.02.027

Cunningham, M.J., Hodgson, S., Masson, D.G., Parson, L.M., 2005. An evaluation of along- and down-slope sediment transport processes between Goban Spur and Brenot Spur on the Celtic Margin of the Bay of Biscay. Sediment. Geol. 179, 99–116. https://doi.org/10.1016/j.sedgeo.2005.04.014

Daly, E., Johnson, M.P., Wilson, A.M., Gerritsen, H.D., Kiriakoulakis, K., Allcock, A.L., White, M., 2018. Bottom trawling at Whittard Canyon: Evidence for seabed modification, trawl plumes and food source heterogeneity. Prog. Oceanogr. 169, 227–240. https://doi.org/10.1016/j.pocean.2017.12.010

de Graciansky, P.C., Poag, C.W., Cunningham, R., Loubere, P., Masson, D.G., Mazzullo, J.M., Montadert, L., Müller, C., Otsuka, K., Reynolds, L., Sigal, J., Snyder, S., Townsend, H.A., Vaos, S.P., Waples, D., 1984. Site 548, in: de Graciansky, P.C., Poag, C.W., Cunningham, R., Loubere, P., Masson, D.G., Mazzullo, J.M., Montadert, L., Müller, C., Otsuka, K., Reynolds, L., Sigal, J., Snyder, S., Townsend, H.A., Vaos, S.P., Waples, D. (Eds.), Initial Reports DSDP, 80. pp. 33–122.

De Mol, B., Van Rensbergen, P., Pillen, S., Van Herreweghe, K., Van Rooij, D., McDonnell, A., Huvenne, V.A.I., Ivanov, M.K., Swennen, R., Henriet, J.-P., 2002. Large deep-water coral banks in the Porcupine Basin, southwest of Ireland. Mar. Geol. 188, 193–231. https://doi.org/10.1016/s0025-3227(02)00281-5

De Mol, L., Van Rooij, D., Pirlet, H., Greinert, J., Frank, N., Quemmerais, F., Henriet, J.P., 2011. Cold-water coral habitats in the Penmarc'h and Guilvinec Canyons (Bay of Biscay): Deep-water versus shallow-water settings. Mar. Geol. 282, 40-52. https://doi.org/10.1016/j.margeo.2010.04.011

Delivet, S., Van Eetvelt, B., Monteys, X., Ribó, M., Van Rooij, D., 2016. Seismic geomorphological reconstructions of Plio-Pleistocene bottom current variability at Goban Spur. Mar. Geol. 378, 261–275. https://doi.org/10.1016/j.margeo.2016.01.001

Deptuck, M.E., Steffens, G.S., Barton, M., Pirmez, C., 2003. Architecture and evolution of upper fan channel-belts on the Niger Delta slope and in the Arabian Sea. Mar. Pet. Geol. 20, 649–676. https://doi.org/10.1016/j.marpetgeo.2003.01.004

Deptuck, M.E., Sylvester, Z., Pirmez, C., O'Byrne, C., 2007. Migration-aggradation history and 3-D seismic geomorphology of submarine channels in the Pleistocene Benin-major Canyon, western Niger Delta slope. Mar. Pet. Geol. 24, 406–433. https://doi.org/10.1016/j.marpetgeo.2007.01.005

Dorschel, B., Hebbeln, D., Foubert, A., White, M., Wheeler, A.J., 2007. Hydrodynamics and cold-water coral facies distribution related to recent sedimentary processes at Galway Mound west of Ireland. Mar. Geol. 244, 184–195. https://doi.org/10.1016/j.margeo.2007.06.010

Ercilla, G., Alonso, B., Wynn, R.B., Baraza, J., 2002. Turbidity current sediment waves on irregular slopes: observations from the Orinoco sediment-wave field. Mar. Geol. 192, 171-187. https://doi.org/10.1016/S0025-3227(02)00554-6

Expedition Scientists, 2005. Modern carbonate mounds: Porcupine drilling. IODP Prelim. Rep. 307.

Faugères, J.-C., Mulder, T., 2011. Contour currents and contourite drifts, in: Developments in Sedimentology. pp. 149–214. https://doi.org/10.1016/B978-0-444-53000-4.00003-2

Faugères, J.C., Gonthier, E., Mulder, T., Kenyon, N., Cirac, P., Griboulard, R., Berné, S., Lesuavé, R., 2002. Multi-process generated sediment waves on the Landes Plateau (Bay of Biscay, North Atlantic). Mar. Geol. 182, 279–302. https://doi.org/10.1016/S0025-3227(01)00242-0

Flood, R.D., 1988. A lee-wave model for deep-sea mudwave activity. Deep. Res. 35, 973–983.

Foubert, A., Henriet, J.-P., 2009. Nature and significance of the recent carbonate mound record: The Mound Challenger Code. Springer Science & Business Media.

Hall, R.A., Aslam, T., Huvenne, V.A.I., 2017. Partly standing internal tides in a dendritic submarine canyon observed by an ocean glider. Deep. Res. Part I Oceanogr. Res. Pap. 126, 73–84. https://doi.org/10.1016/j.dsr.2017.05.015

Harris, P.T., Macmillan-Lawler, M., Rupp, J., Baker, E.K., 2014. Geomorphology of the oceans. Mar. Geol. 352, 4–24. https://doi.org/10.1016/j.margeo.2014.01.011

Harris, P.T., Whiteway, T., 2011. Global distribution of large submarine canyons: Geomorphic differences between active and passive continental margins. Mar. Geol. 285, 69–86. https://doi.org/10.1016/j.margeo.2011.05.008

Hernández-Molina, F.J., Stow, D.A.V., Alvarez-Zarikian, C.A., Acton, G., Bahr, A., Balestra, B., Ducassou, E., Flood, R., Flores, J.A., Furota, S., Grunert, P., Hodell, D., Jimenez-Espejo, F., Kim, J.K., Krissek, L., Kuroda, J., Li, B., Llave, E., Lofi, J., Lourens, L., Miller, M., Nanayama, F., Nishida, N., Richter, C., Roque, C., Pereira, H., Sanchez Goñi, M.F., Sierro, F.J., Singh, A.D., Sloss, C., Takashimizu, Y., Tzanova, A., Voelker, A., Willimas, T., Xuan, C., 2014. Onset of Mediterranean outflow into the North Atlantic. Science 344, 1244-1250. https://doi.org/10.1126/science.1251306

Hovland, M., Gardner, J.V., Judd, A.G., 2002. The significance of pockmarks to understanding fluid flow processes and geohazards. Geofluids 2, 127–136.

Hovland, M., Judd, A.G., 1988. Seabed Pockmarks and Seepages: Impact on Geology, Biology, and the Marine Environment. London: Graham & Trotman.

Huvenne, V.A.I., Tyler, P.A., Masson, D.G., Fisher, E.H., Hauton, C., Hühnerbach, V., Le Bas, T.P., Wolff, G.A., 2011. A picture on the wall: Innovative mapping reveals cold-water coral refuge in submarine canyon. PLoS One 6, e28755. https://doi.org/10.1371/journal.pone.0028755

Huvenne, V.A.I., Van Rooij, D., De Mol, B., Thierens, M., O'Donnell, R., Foubert, A., 2009. Sediment dynamics and palaeo-environmental context at key stages in the Challenger cold-water coral mound formation: Clues from sediment deposits at the mound base. Deep. Res. Part I Oceanogr. Res. Pap. 56, 2263–2280. https://doi.org/10.1016/j.dsr.2009.08.003

Judd, A.G., Hovland, M., 2009. Seabed Fluid Flow - Impact of geology, biology and the marine environment. Cambridge University Press.

Kano, A., Ferdelman, T.G., Williams, T., Henriet, J.-P., Ishikawa, T., Kawagoe, N., Talkashima, C., Kakizaki, Y., Abe, K., Sakai, S., Browning, E.L., Li, X., The IODP Expedition 307 Scientific Party, 2007. Age constraints on the origin and growth history of a deep-water coral mound in the northeast Atlantic drilled during Integrated Ocean Drilling Program Expedition 307. Geology 35, 1051–1054.

Kenyon, N.H., Belderson, R.H., Stride, A.H., 1978. Channels, canyons and slump folds on the continental slope between South-West lreland and Spain. Oceanol. Acta 1, 369–380.

Kenyon, N.H., Ivanov, M.K., Akhmetzhanov, A.M., 1998. Cold water carbonate mounds and sediment transport on the Northeast Atlantic margin. IOC Tech. Ser. 52.

Khélifi, N., Sarnthein, M., Andersen, N., Blanz, T., Frank, M., Garbe-Schönberg, D., Haley, B.A., Stumpf, R., Weinelt, M., 2009. A major and long-term Pliocene intensification of the Mediterranean outflow, 3.5-3.3 Ma ago. Geology 37, 811–814. https://doi.org/10.1130/G30058A.1

King, L.H., MacLean, B., 1970. Pockmarks on the Scotian Shelf. Geol. Soc. Am. Bull. 81, 3141–3148.

Kolla, V., Ravindranathan, R., Gupta, P., Mathur, M., Sinha, N., 2021. Distribution, characteristics, and processes of formation of sediment waves along the Indian north-eastern continental margin. Mar.

Geol. 441, 106597. https://doi.org/10.1016/j.margeo.2021.106597

Lamb, K.G., 2014. Internal wave breaking and dissipation mechanisms on the continental slope/shelf. Annu. Rev. Fluid Mech. 46, 231–254. https://doi.org/10.1146/annurev-fluid-011212-140701

Lambeck, K., 1996. Glaciation and sea-level change for Ireland and the Irish Sea since Late Devensian/Midlandian time. J. Geol. Soc. London 153, 853–872.

Lee, H.J., Syvitski, J.P.M., Parker, G., Orange, D., Locat, J., Hutton, E.W.H., Imran, J., 2002. Distinguishing sediment waves from slope failure deposits: Field examples, including the "Humboldt slide", and modelling results. Mar. Geol. 192, 79–104. https://doi.org/10.1016/S0025-3227(02)00550-9

Lim, A., Huvenne, V.A.I., Vertino, A., Spezzaferri, S., Wheeler, A.J., 2018. New insights on coral mound development from groundtruthed high-resolution ROV-mounted multibeam imaging. Mar. Geol. 403, 225–237. https://doi.org/10.1016/j.margeo.2018.06.006

Louwye, S., Foubert, A., Mertens, K., Van Rooij, D., The IODP Expedition 307 Scientific Party, 2008. Integrated stratigraphy and palaeoecology of the Lower and Middle Miocene of the Porcupine Basin. Geol. Mag. 145, 321–344. https://doi.org/10.1017/S0016756807004244

Maier, K.L., Rosenberger, K.J., Paull, C.K., Gwiazda, R., Gales, J., Lorenson, T., Barry, J.P., Talling, P.J., McGann, M., Xu, J., Lundsten, E., Anderson, K., Litvin, S.Y., Parsons, D.R., Clare, M.A., Simmons, S.M., Sumner, E.J., Cartigny, M.J.B., 2019. Sediment and organic carbon transport and deposition driven by internal tides along Monterey Canyon, offshore California. Deep. Res. Part I Oceanogr. Res. Pap. 153, 103108. https://doi.org/10.1016/j.dsr.2019.103108

Marchès, E., Mulder, T., Cremer, M., Bonnel, C., Hanquiez, V., Gonthier, E., Lecroart, P., 2007. Contourite drift construction influenced by capture of Mediterranean Outflow Water deep-sea current by the Portimão submarine canyon (Gulf of Cadiz, South Portugal). Mar. Geol. 242, 247-260. https://doi.org/10.1016/j.margeo.2007.03.013

Masson, D.G., Howe, J.A., Stoker, M.S., 2002. Bottom-current sediment waves, sediment drifts and contourites in the northern Rockall Trough. Mar. Geol. 192, 215–237. https://doi.org/10.1016/S0025-3227(02)00556-X

McCann, T., Shannon, P.M., Moore, J.G., 1995. Fault styles in the Porcupine Basin, offshore Ireland: tectonic and sedimentary controls. Geol. Soc. London, Spec. Publ. 93, 371–383. https://doi.org/10.1144/gsl.sp.1995.093.01.29

McCave, I.N., 2017. Formation of sediment waves by turbidity currents and geostrophic flows: A discussion. Mar. Geol. 390, 89–93. https://doi.org/10.1016/j.margeo.2017.05.003

McDonnell, A., Shannon, P.M., 2001. Comparative Tertiary stratigraphic evolution of the Porcupine and Rockall basins. Geol. Soc. London, Spec. Publ. 188, 323–344.

Mestdagh, T., Lobo, F.J., Llave, E., Hernández-Molina, F.J., García Ledesma, A., Puga-Bernabéu, Á., Fernández-Salas, L.-M., Van Rooij, D., 2020. Late Quaternary multi-genetic processes and products on the northern Gulf of Cadiz upper continental slope (SW Iberian Peninsula). Mar. Geol. 427, 106214. https://doi.org/10.1016/j.margeo.2020.106214

Micallef, A., Mountjoy, J.J., Canals, M., Lastras, G., 2012. Deep-Seated Bedrock Landslides and Submarine Canyon Evolution in an Active Tectonic Margin: Cook Strait, New Zealand, in: Yamada, Y., Kawamura, K., Ikehara, K., Ogawa, Y., Urgeles, R., Mosher, D., Chaytor, J., Strasser, M. (Eds.), Submarine Mass Movements and Their Consequences. Springer Netherlands, Dordrecht, pp. 201–212. https://doi.org/10.1007/978-94-007-2162-3_18

Mienis, F., de Stigter, H.C., de Haas, H., van Weering, T.C.E., 2009. Near-bed particle deposition and resuspension in a cold-water coral mound area at the Southwest Rockall Trough margin, NE Atlantic. Deep. Res. Part I Oceanogr. Res. Pap. 56, 1026–1038. https://doi.org/10.1016/j.dsr.2009.01.006

Migeon, S., Savoye, B., Faugeres, J.-C., 2000. Quaternary development of migrating sediment waves in the Var deep-sea fan: Distribution, growth pattern, and implication for levee evolution. Sediment. Geol. 133, 265–293. https://doi.org/10.1016/S0037-0738(00)00043-9

Moernaut, J., Wiemer, G., Reusch, A., Stark, N., De Batist, M., Urrutia, R., Ladrón de Guevara, B., Kopf, A., Strasser, M., 2017. The influence of overpressure and focused fluid flow on subaquatic slope stability in a formerly glaciated basin: Lake Villarrica (South-Central Chile). Mar. Geol. 383, 35–54. https://doi.org/10.1016/j.margeo.2016.11.012

Moore, J.G., Shannon, P.M., 1992. Palaeocene-Eocene deltaic sedimentation, Porcupine Basin, offshore Ireland - a sequence stratigraphic approach. First Break 10, 461–469. https://doi.org/10.3997/1365-2397.1992024

Morozov, E.G., Pisarev, S.V., 2002. Internal tides at the Arctic latitudes (numerical experiments). Oceanology 42, 153-161.

Mountjoy, J.J., Howarth, J.D., Orpin, A.R., Barnes, P.M., Bowden, D.A., Rowden, A.A., Schimel, A.C.G., Holden, C., Horgan, H.J., Nodder, S.D., Patton, J.R., Lamarche, G., Gerstenberger, M., Micallef, A., Pallentin, A., Kane, T., 2018. Earthquakes drive large-scale submarine canyon development and sediment supply to deep-ocean basins. Sci. Adv. 4. https://doi.org/10.1126/sciadv.aar3748

Mulder, T., 2011. Gravity processes and deposits on continental slope, rise and abyssal plains, in: Developments in Sedimentology. Elsevier, pp. 25–148. https://doi.org/10.1016/B978-0-444-53000-4.00002-0

Mulder, T., Zaragosi, S., Garlan, T., Mavel, J., Cremer, M., Sottolichio, A., Sénéchal, N., Schmidt, S., 2012. Present deep-submarine canyons activity in the Bay of Biscay (NE Atlantic). Mar. Geol. 295–298, 113–127. https://doi.org/10.1016/j.margeo.2011.12.005

Naylor, D., Shannon, P., 1982. Porcupine Basin, in: Naylor, D., Shannon, P. (Eds.), Geology of Offshore Ireland and West Britain. Graham & Trotman, pp. 67–75. https://doi.org/10.1007/978-94-010-9358-3_7

Naylor, D., Shannon, P.M., 2005. The structural framework of the Irish Atlantic Margin, in: Doré, A.G., Vining, B.A. (Eds.), Petroleum Geology: North-West Europe and Global Perspectives - Proceedings of the 6th Petroleum Geology Conference. Geological Society, London, pp. 1009–1021.

Normark, W.R., Piper, D.J.W., Posamentier, H., Pirmez, C., Migeon, S., 2002. Variability in form and growth of sediment waves on turbidite channel levees, Marine Geology. https://doi.org/10.1016/S0025-3227(02)00548-0

Pingree, R.D., Le Cann, B., 1990. Structure, strength and seasonality of the slope currents in the Bay of Biscay region. J. Mar. Biol. Assoc. United Kingdom 70, 857–885. https://doi.org/10.1017/S0025315400059117

Pingree, R.D., Le Cann, B., 1989. Celtic and Armorican slope and shelf residual currents. Prog. Oceanogr. 23, 303–338. https://doi.org/10.1016/0079-6611(89)90003-7

Piper, D.J.W., Normark, W.R., 2009. Processes that initiate turbidity currents and their influence on turbidites: A marine geology perspective. J. Sediment. Res. 79, 347–362. https://doi.org/10.2110/jsr.2009.046

Pomar, L., Morsilli, M., Hallock, P., Bádenas, B., 2012. Internal waves, an under-explored source of turbulence events in the sedimentary record. Earth-Sci. Rev. 111, 56-81. https://doi.org/10.1016/j.earscirev.2011.12.005

Puig, P., Palanques, A., Martín, J., 2014. Contemporary sediment-transport processes in submarine canyons. Ann. Rev. Mar. Sci. 6, 53–77. https://doi.org/10.1146/annurev-marine-010213-135037

Raddatz, J., Rüggeberg, A., Liebetrau, V., Foubert, A., Hathorne, E.C., Fietzke, J., Eisenhauer, A., Dullo, W.C., 2014. Environmental boundary conditions of cold-water coral mound growth over the last 3 million years in the Porcupine Seabight, Northeast Atlantic. Deep Sea Rese. Part II Top. Stud. Oceanogr 99, 227-236. https://doi.org/10.1016/j.dsr2.2013.06.009

Ribó, M., Puig, P., Muñoz, A., Lo Iacono, C., Masqué, P., Palanques, A., Acosta, J., Guillén, J., Gómez Ballesteros, M., 2016. Morphobathymetric analysis of the large fine-grained sediment waves over the Gulf of Valencia continental slope (NW Mediterranean). Geomorphology 253, 22–37. https://doi.org/10.1016/j.geomorph.2015.09.027

Rice, A.L., Billett, D.S.M., Thurston, M.H., Lampitt, R.S., 1991. The Institute of Oceanographic Sciences Biology Programme in the Porcupine Seabight: Background and general introduction. J. Mar. Biol. Assoc. United Kingdom 71, 281–310. https://doi.org/10.1017/S0025315400051614

Rice, A.L., Thurston, M.H., New, A.L., 1990. Dense aggregations of a hexactinellid sponge, Pheronema carpenteri, in the Porcupine Seabight (northeast Atlantic Ocean), and possible causes. Prog. Oceanogr. 24, 179–196.

Schlitzer, R., 2020. Ocean Data View [WWW Document].

Scourse, J.D., Chiverrell, R., Smedley, R., Small, D., Burke, M., Saher, M., Van Landeghem, K., Duller, G.A.T., Ó Cofaigh, C., Bateman, M., Benetti, S., Bradley, S.L., Callard, S.L., Evans, D., Fabel, D., Mc Carron, S., Medialdea, A., Moreton, S., Ou, X., Praeg, D., Roberts, D., Roberts, H.M., Clark, C., 2021. Maximum extent and readvance dynamics of the Irish Sea Ice Stream and Irish Sea Glacier since the Last Glacial. J. Quat. Sci. 36, 780-804. https://doi.org/10.1002/jqs.3313

Scourse, J.D., Hall, I.R., McCave, I.N., Young, J.R., Sugdon, C., 2000. The origin of Heinrich layers: Evidence from H2 for European precursor events. Earth Planet. Sci. Lett. 182, 187–195. https://doi.org/10.1016/S0012-821X(00)00241-7

Scourse, J.D., Uehara, K., Wainwright, A., 2009. Celtic Sea linear tidal sand ridges, the Irish Sea Ice Stream and the Fleuve Manche: Palaeotidal modelling of a transitional passive margin depositional system. Mar. Geol. 259, 102–111. https://doi.org/10.1016/j.margeo.2008.12.010

Sejrup, H.P., Hjelstuen, B.O., Dahlgren, K.I.T., Haflidason, H., Kuijpers, A., Nygård, A., Praeg, D., Stoker, M.S., Vorren, T.O., 2005. Pleistocene glacial history of the NW European continental margin. Mar. Pet. Geol. 22, 1111–1129. https://doi.org/10.1016/j.marpetgeo.2004.09.007

Shanmugam, G., 2013. Modem internal waves and internal tides along oceanic pycnoclines: Challenges and implications for ancient deep-marine baroclinic sands. Am. Assoc. Pet. Geol. Bull. 97, 799–843. https://doi.org/10.1306/10171212101

Shannon, P.M., 1991. The development of Irish offshore sedimentary basins. J. Geol. Soc. London. 148, 181–189. https://doi.org/10.1144/gsjgs.148.1.0181

Shannon, P.M., McDonnell, A., Bailey, W.R., 2007. The evolution of the Porcupine and Rockall basins, offshore Ireland: the geological template for carbonate mound development. Int. J. Earth Sci. 96, 21–35. https://doi.org/10.1007/s00531-006-0081-y

Shepard, F.P., 1965. Types of submarine valleys. Am. Assoc. Pet. Geol. Bull. 49, 304–310. https://doi.org/10.1017/CBO9781107415324.004

Stewart, H.A., Davies, J.S., Guinan, J., Howell, K.L., 2014. The Dangeard and Explorer canyons, South Western Approaches UK: Geology, sedimentology and newly discovered cold-water coral mini-mounds. Deep. Res. Part II Top. Stud. Oceanogr. 104, 230–244. https://doi.org/10.1016/j.dsr2.2013.08.018

Stoker, M.S., Praeg, D., Hjelstuen, B.O., Laberg, J.S., Nielsen, T., Shannon, P.M., 2005. Neogene stratigraphy and the sedimentary and oceanographic development of the NW European Atlantic margin. Mar. Pet.

Geol. 22, 977–1005. https://doi.org/10.1016/j.marpetgeo.2004.11.007

Stoker, M.S.S., Van Weering, T.C.E., Svaerdborg, T., 2001. A Mid- to Late Cenozoic tectonostratigraphic framework for the Rockall Trough. Geol. Soc. London, Spec. Publ. 188, 411–438. https://doi.org/10.1144/GSL.SP.2001.188.01.26

Stow, D.A.V., Faugères, J.-C., Howe, J.A., Pudsey, C.J., Viana, A.R., 2002. Bottom currents, contourites and deep-sea sediment drifts: Current state-of-the-art. Geol. Soc. 22, 7–20. https://doi.org/10.1144/GSL.MEM.2002.022.01.02

Symons, W.O., Sumner, E.J., Talling, P.J., Cartigny, M.J.B., Clare, M.A., 2016. Large-scale sediment waves and scours on the modern seafloor and their implications for the prevalence of supercritical flows. Mar. Geol. 371, 130–148. https://doi.org/10.1016/j.margeo.2015.11.009

Thierens, M., Browning, E., Pirlet, H., Loutre, M.-F., Dorschel, B., Huvenne, V.A.I.A.I., Titschack, J., Colin, C., Foubert, A., Wheeler, A.J., 2013. Cold-water coral carbonate mounds as unique palaeo-archives: The Plio-Pleistocene Challenger Mound record (NE Atlantic). Quat. Sci. Rev. 73, 14–30. https://doi.org/10.1016/j.quascirev.2013.05.006

Thierens, M., Titschack, J., Dorschel, B., Huvenne, V.A.I., Wheeler, A.J., Stuut, J.-B., O'Donnell, R., 2010. The 2.6 Ma depositional sequence from the Challenger cold-water coral carbonate mound (IODP Exp. 307): Sediment contributors and hydrodynamic palaeo-environments. Mar. Geol. 271, 260–277. https://doi.org/10.1016/j.margeo.2010.02.021

Toucanne, S., Soulet, G., Riveiros, N.V., Boswell, S.M., Dennielou, B., Waelbroeck, C., Bayon, G., Mojtahid, M., Bosq, M., Sabine, M., Zaragosi, S., Bourillet, J.F., Mercier, H., 2021. The North Atlantic Glacial Eastern Boundary Current as a key driver for ice-sheet-AMOC interactions and climate instability. Paleoceanogr. Paleoclimatol. 36, e2020PA004068. https://doi.org/10.1029/2020PA004068

Toucanne, S., Zaragosi, S., Bourillet, J.F., Naughton, F., Cremer, M., Eynaud, F., Dennielou, B., 2008. Activity of the turbidite levees of the Celtic-Armorican margin (Bay of Biscay) during the last 30,000 years: Imprints of the last European deglaciation and Heinrich events. Mar. Geol. 247, 84–103. https://doi.org/10.1016/j.margeo.2007.08.006

Tudhope, A.W., Scoffin, T.P., 1995. Processes of sedimentation in Gollum Channel, Porcupine Seabight: Submersible observations and sediment analyses. Trans. R. Soc. Edinb. Earth Sci. 86, 49–55. https://doi.org/10.1017/S0263593300002157

Van Aken, H.M., 2000. The hydrography of the mid-latitude northeast Atlantic Ocean I: The deep water masses. Deep. Res. Part I Oceanogr. Res. Pap. 47, 757–788. https://doi.org/10.1016/S0967-0637(99)00092-8

Van Rooij, D., 2004. An integrated study of Quaternary sedimentary processes on the eastern slope of the Porcupine Seabight, SW of Ireland. Unpubl. Dr. Diss. Ghent Univ. Belgium.

Van Rooij, D., Blamart, D., Kozachenko, M., Henriet, J.-P., 2007a. Small mounded contourite drifts associated with deep-water coral banks, Porcupine Seabight, NE Atlantic Ocean. Geol. Soc. London, Spec. Publ. 276, 225–244. https://doi.org/10.1144/gsl.sp.2007.276.01.11

Van Rooij, D., Blamart, D., Richter, T., Wheeler, A.J., Kozachenko, M., Henriet, J.-P., 2007b. Quaternary sediment dynamics in the Belgica mound province, Porcupine Seabight: ice-rafting events and contour current processes. Int. J. Earth Sci. 96, 121–140. https://doi.org/10.1007/s00531-006-0086-6

Van Rooij, D., De Mol, B., Huvenne, V.A.I., Ivanov, M.K., Henriet, J.-P., 2003. Seismic evidence of current-controlled sedimentation in the Belgica mound province, upper Porcupine slope, southwest of Ireland. Mar. Geol. 195, 31–53. https://doi.org/10.1016/s0025-3227(02)00681-3

Van Rooij, D., Foubert, A., Nys, M., Blamart, D., Kozachenko, M., Henriet, J.-P., 2002. A multi-disciplinary study of Late-Caenozoic sedimentary processes on the eastern slope of the Porcupine Seabight, southwest of Ireland, in: Degryse, P., Sintubin, M. (Eds.), Contributions to the Geology of Belgium and Northwest Europe: Proceedings of the First Geologica Belgica International Meeting, Leuven, 11-15 September 2002. Aardkundige Mededelingen, 12. pp. 59–62.

Van Rooij, D., Huvenne, V.A.I., Blamart, D., Henriet, J.-P., Wheeler, A.J., de Haas, H., 2009. The Enya mounds: A lost mound-drift competition. Int. J. Earth Sci. 98, 849–863. https://doi.org/10.1007/s00531-007-0293-9

Waterhouse, A.F., Mackinnon, J.A., Musgravea, R.C., Kelly, S.M., Pickering, A., Nash, J., 2017. Internal tide convergence and mixing in a submarine canyon. J. Phys. Oceanogr. 47, 303–322. https://doi.org/10.1175/JPO-D-16-0073.1

Watson, S.J., Mountjoy, J.J., Crutchley, G., 2020. Tectonic and geomorphic controls on the distribution of submarine landslides across active and passive margins, eastern New Zealand. Geol. Soc. London, Spec. Publ. 500, 477–494. https://doi.org/https://doi.org/10.1144/SP500-2019-165 Received

Weatherall, P., Marks, K.M., Jakobsson, M., Schmitt, T., Tani, S., Arndt, J.E., Rovere, M., Chayes, D., Ferrini, V., Wigley, R., 2015. A new digital bathymetric model of the world's oceans. Earth Sp. Sci. 2, 331–345.

Weaver, P.P.E., Wynn, R.B., Kenyon, N.H., Evans, J., 2000. Continental margin sedimentation, with special reference to the north-east Atlantic margin. Sedimentology 47, 239–256.

Wheeler, A.J.A.J., Kenyon, N.H.N.H., Ivanov, M.K., Beyer, A., Cronin, B.T.B.T., Schenke, H.W., Akhmetzhanov, A.M., Satur, N., Zaragosi, S., McDonnell, A., Schenke, H.W., Akhmetzhanov, A.M., Satur, N., Zaragosi, S., 2003. Canyon Heads and Channel Architecture of the Gollum Channel, Porcupine Seabight, in: Mienert, J., Weaver, P. (Eds.), European Margin Dynamics. Side-Scan Sonar and Seismic Images. Springer, Berlin, pp. 183–186. https://doi.org/10.1029/2003eo190009

White, M., 2007. Benthic dynamics at the carbonate mound regions of the Porcupine Sea Bight continental margin. Int. J. Earth Sci. 96, 1–9. https://doi.org/10.1007/s00531-006-0099-1

White, M., Dorschel, B., 2010. The importance of the permanent thermocline to the cold water coral carbonate mound distribution in the NE Atlantic. Earth Planet. Sci. Lett. 296, 395–402. https://doi.org/10.1016/j.epsl.2010.05.025

Wienberg, C., Titschack, J., Frank, N., De Pol-Holz, R., Fietzke, J., Eisele, M., Kremer, A., Hebbeln, D., 2020. Deglacial upslope shift of NE Atlantic intermediate waters controlled slope erosion and cold-water coral mound formation (Porcupine Seabight, Irish margin). Quat. Sci. Rev. 237, 106310. https://doi.org/10.1016/j.quascirev.2020.106310

Wilson, A.M., Raine, R., Mohn, C., White, M., 2015. Nepheloid layer distribution in the Whittard Canyon, NE Atlantic Margin. Mar. Geol. 367, 130–142. https://doi.org/10.1016/j.margeo.2015.06.002

Wynn, R.B., Weaver, P.P.E., Ercilla, G., Stow, D.A.V., Masson, D.G., 2000. Sedimentary processes in the Selvage sediment-wave field, NE Atlantic: new insights into the formation of sediment waves by turbidity currents. Sedimentology 47, 1181-1197. https://doi.org/10.1046/j.1365-3091.2000.00348.x

Wynn, R.B., Cronin, B.T., Peakall, J., 2007. Sinuous deep-water channels: Genesis, geometry and architecture. Mar. Pet. Geol. 24, 341–387. https://doi.org/10.1016/j.marpetgeo.2007.06.001

Wynn, R.B., Masson, D.G., 2008. Sediment waves and bedforms, in: Rebesco, M., Camerlenghi, A. (Eds.), Developments in Sedimentology: Contourites. Elsevier, pp. 289–300.

Xu, J.P., Noble, M.A., 2009. Currents in Monterey Submarine Canyon. J. Geophys. Res. Ocean. 114, 1–20. https://doi.org/10.1029/2008JC004992

Zaragosi, S., Auffret, G.A., Faugères, J.-C., Garlan, T., Pujol, C., Cortijo, E., 2000. Physiography and recent sediment distribution of the Celtic Deep-Sea Fan, Bay of Biscay. Mar. Geol. 169, 207–237. https://doi.org/10.1016/S0025-3227(00)00054-2

Zaragosi, S., Bourillet, J.F., Eynaud, F., Toucanne, S., Denhard, B., Van Toer, A., Lanfumey, V., 2006. The impact of the last European deglaciation on the deep-sea turbidite systems of the Celtic-Armorican margin (Bay of Biscay). Geo-Marine Lett. 26, 317–329. https://doi.org/10.1007/s00367-006-0048-9

FIGURE CAPTIONS

Figure 1. (A) Shaded relief bathymetry map showing the location of the Gollum Channel System (GCS; blue shaded area) and Kings Channel System (KCS; green shaded area) within the Porcupine Seabight, southwest of Ireland. The study area is indicated by the dark grey shaded area. The Belgica Mound Province (BMP) and Enya mounds (EM) north of the study area are circled in purple. The Whittard Canyon System on the Celtic Margin is shown in yellow. The European Slope Current (ESC) is indicated with light blue arrows (based on Toucanne et al., 2021). The maximum extent of the British-Irish Ice Sheet (BIIS) at the Last Glacial Maximum (LGM) is indicated as a white shaded area contoured by a grey dotted line (based on Scourse et al., 2021). Contour lines are drawn every 1000 m. The inset map shows the location of the Porcupine Seabight on the NW European continental margin. The regional extent of the ESC is shown in light blue. The bathymetry map is adapted from the GEBCO_2014 grid from General Bathymetric Chart of the Oceans (GEBCO; Weatherall et al., 2015). (B) Coloured bathymetry map of the study area (Beyer et al., 2003), with the thalwegs of the four channels under investigation here indicated in blue and with contour lines drawn every 200 m. Also indicated are the seismic profiles available for this study. The purple dots indicate the locations of two moorings, one of which is mooring 112 from Pingree and Le Cann (1990). The blue star indicates the location of the CTD cast that was used for Fig. 11. (C) Close-up slope angle map of the KCS with indication of the Denethor area (DA; encircled in black), the crests of sediment waves (solid black lines), three internal levees (dashed black lines), and the head- and/or or sidewall scarps of two slope failures (dotted black lines): one at the edge of the Denethor area and one on the southern flank of Theoden Channel. (D) Close-up slope angle map (same legend as in (C)) of the two northernmost channels of the GCS with indication of a scarp north of Bilbo Channel (dotted black line) and sudden changes in orientation in both channels (black circles) seemingly lining up (black dashed lines). (E) Close-up slope angle map of a section of the pockmark (PM) field north of Theoden Channel. The channels in (B)-(D) are labelled as follows: AC = Aragorn Channel, TC = Theoden Channel, BC = Bilbo Channel, FC = Frodo Channel. The grey background maps in (B)-(D) are composed from data from the Irish National Seabed Survey.

Figure 2. Salinity versus depth profile of a section within the Porcupine Seabight crossing the eastern slope in between the KCS and GCS (location: see Fig. 1A), based on CTD data (blue triangles) of the World Ocean Database (Boyer et al., 2018) and produced using Ocean Data View (Schlitzer, 2020). The white zone near the slope between 1000 and 1500 m water depth is due to a lack of data in that area. Salinity contour lines are drawn every 0.1. The depth range of the sediment waves occurring north of Theoden Channel is indicated by the white arrow. Also added (in white text) are the different water masses present: ENACW = Eastern North Atlantic Central Water, MOW = Mediterranean Outflow Water, LSW = Labrador Sea Water, NEADW = North East Atlantic Deep Water, NSW = Norwegian Sea Water. Internal waves, indicated in grey, can occur at the interface between ENACW and MOW (White, 2007).

Figure 3. Sketch showing the definitions of channel dimensions used in the bathymetry analysis.

Figure 4. (A) Seismic profile (location: see Fig. 1B) crossing Aragorn Channel and a smaller channel in the KCS with (B) interpretation indicating the seismic stratigraphic units and their boundaries as described in the text. PM indicates the locations of pockmarks recognized on the profile. The orange arrow in unit SUa indicates a southward progradation of reflectors. The blue arrows in units SUa and SUb indicate on- or downlap onto the LD1a and LD1b surfaces, respectively. Grey shaded areas indicate zones with chaotic or transparent seismic facies in the channel infill.

Figure 5. (A) Seismic profile (location: see Fig. 1B) crossing Theoden Channel in the KCS with (B) interpretation indicating the seismic stratigraphic units and their boundaries as described in the text. Grey shaded areas indicate zones with chaotic or transparent seismic facies in the channel infill. PM indicates the locations of pockmarks recognized on the profile.

Figure 6. (A) Seismic profile (location: see Fig. 1B) crossing the slope north of Aragorn Channel in the KCS with (B) interpretation indicating the seismic stratigraphic units and their boundaries as described in the text. The orange arrows indicate upslope migration of wavy reflectors in unit SUa. The blue arrows in unit U1 indicate onlap onto the RD1 reflector. The blue arrows in units SUa and SUb indicate on- or downlap onto the LD1a and LD1b surfaces, respectively. PM indicates the locations of pockmarks recognized on the profile.

Figure 7. (A) Seismic profile (location: see Fig. 1B) crossing Bilbo and Frodo channels in the GCS with (B) interpretation indicating the seismic stratigraphic units and their boundaries as described in the text. Grey shaded areas indicate zones with chaotic or transparent seismic facies in the channel infill.

Figure 8. (A) Seismic profile (location: see Fig. 1B) crossing Bilbo Channel in the GCS with (B) interpretation indicating the seismic stratigraphic units and their boundaries as described in the text. The blue arrow in the middle of the figure indicates truncation by an internal reflection.

Figure 9. (A) Seismic profile (location: see Fig. 1B) crossing the Denethor area and the sediment wave field north of Theoden Channel in the KCS with (B) interpretation indicating the seismic stratigraphic units and their boundaries as described in the text. PM indicates the locations of pockmarks recognized on the profile. The grey shaded area at the base of the slope indicates a zone with transparent seismic facies. The white arrows indicate the migration of sediment wave crests. The blue arrows in U2 indicate onlapping.

Figure 10. Data from the mooring in Bilbo Channel (location: Fig. 1B) spanning the period from mid-June to mid-December 2005. (A) Time series of the daily mean current speed. (B) Time series of the instantaneous current speed. The grey arrows indicate long-term cyclicity. (C) Close-up shaded bathymetry map of the uppermost section of Bilbo Channel (BC; colour scale and location: Figs. 1B, 1D), with indication of the location of the mooring (blue circle), the residual current vector (white arrow), and the major axis of the M_2 tidal ellipse (black arrow). (D) Histogram of the instantaneous current speed measurements. (E) Close-up time series of the instantaneous current speed. The grey arrows indicate spring-neap cyclicity.

Figure 11. (A) Ratio of the slope angle (γ) to the angle of energy propagation of internal waves (c) over the present-day seabed in the sediment wave field at the location of the seismic profile shown in Fig. 9 (location: see Fig. 1B). The extent of the sediment wave field in the study area is indicated by the arrow. The permanent thermocline, roughly coinciding with the interface between ENACW (= Eastern North Atlantic Central Water) and MOW (= Mediterranean Outflow Water), is indicated by a white dashed line. (B) Graphs of the Brunt-Väisälä frequency (blue) and the slope angle (red) versus depth from the WOD18 (Boyer et al., 2018) CTD station between the KCS and GCS (location: see Fig. 1B) and from the bathymetry profile in (A), respectively.

TABLE CAPTION

Table 1. Main technical specifications of the seismic reflection acquisition during each of the RV Belgica campaigns.

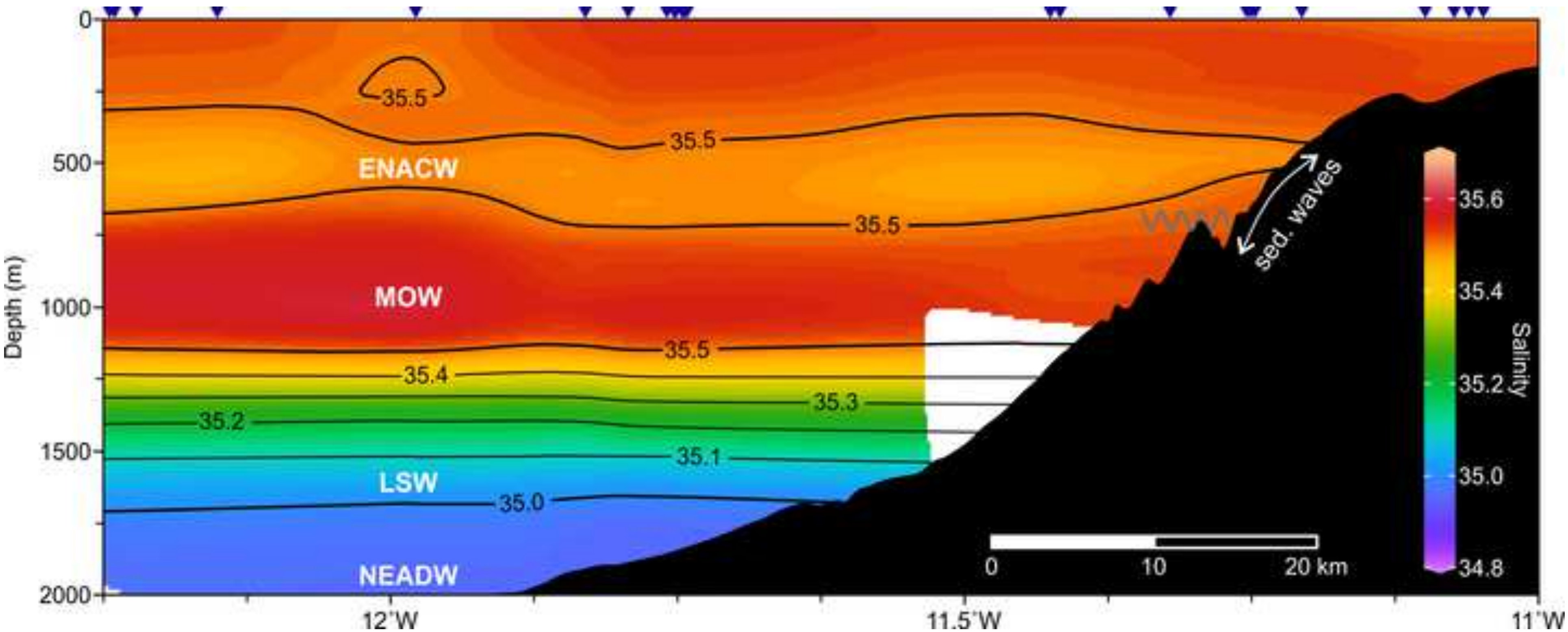

0
500
1000
1500
2000
Depth (m)
35.5
35.5
35.5
35.5
35.4
35.3
35.2
35.1
35.0
ENACW
MOW
LSW
NEADW
sed. waves
0
10
20 km
35.6
35.4
35.2
35.0
34.8
Salinity
12°W
11.5°W
11°W

Figure3

Click here to access/download;Figure;FIG3.tif

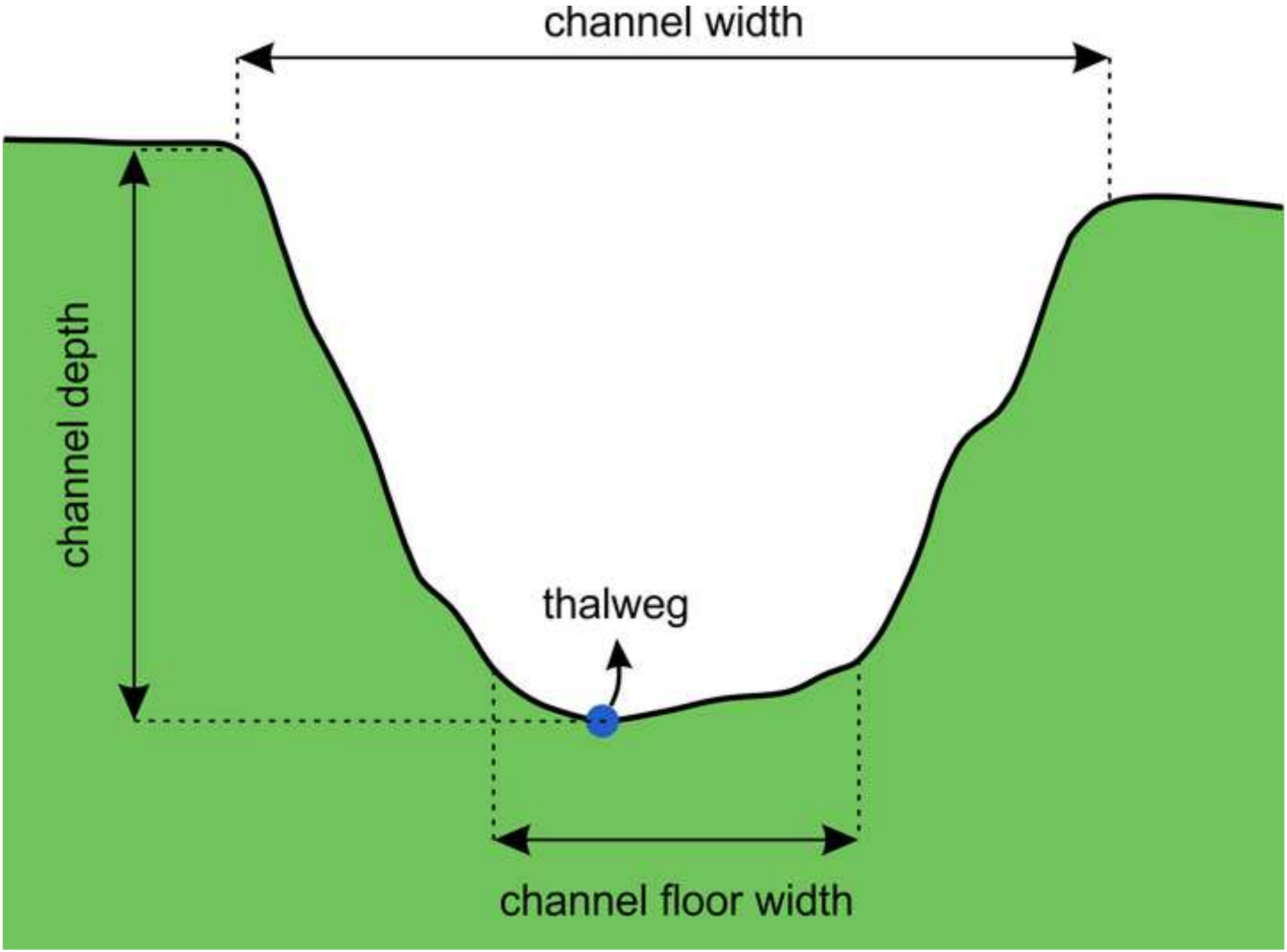

Figure5

Click here to access/download;Figure;FIG5.tif

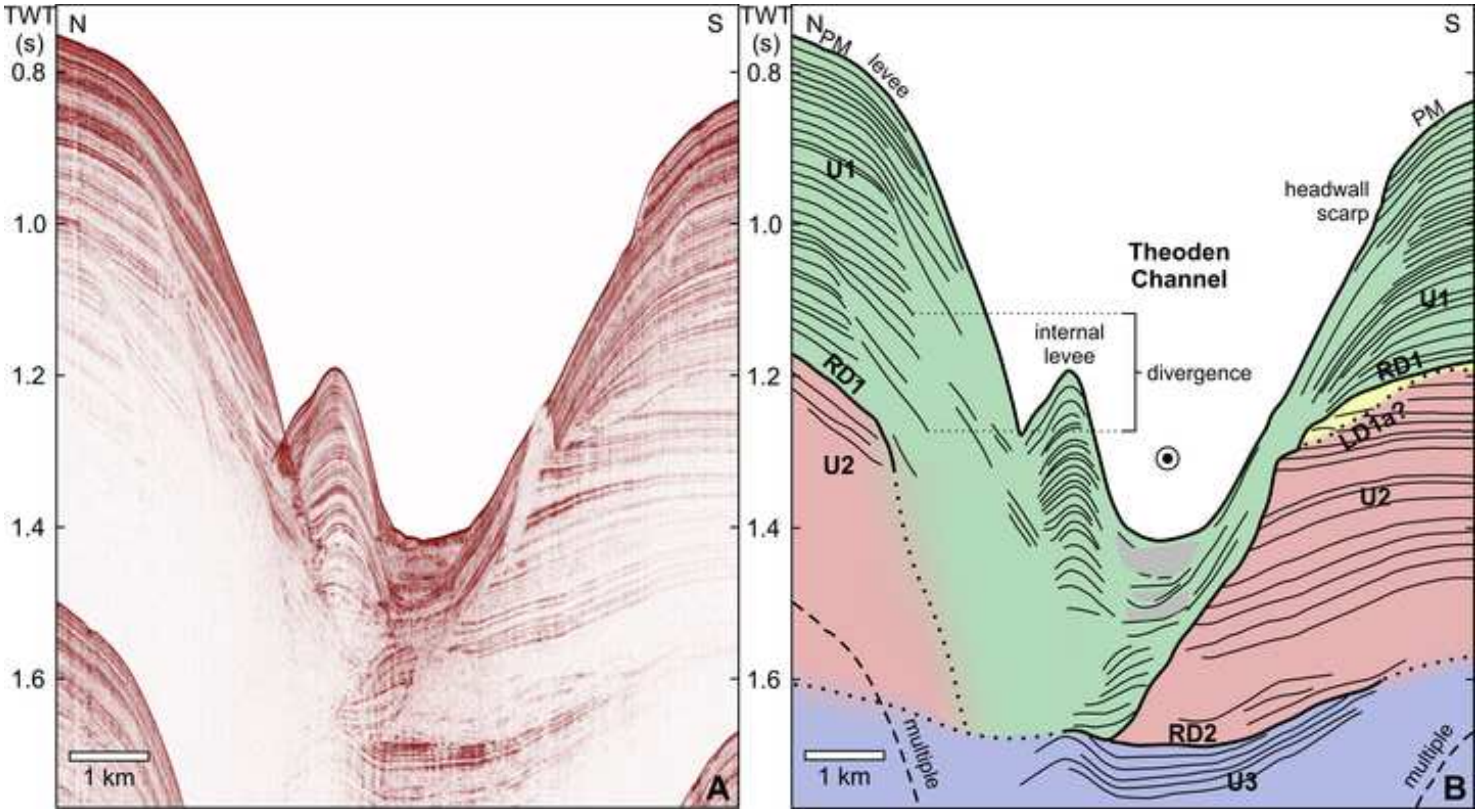

Figure7

Click here to access/download;Figure;FIG7.tif

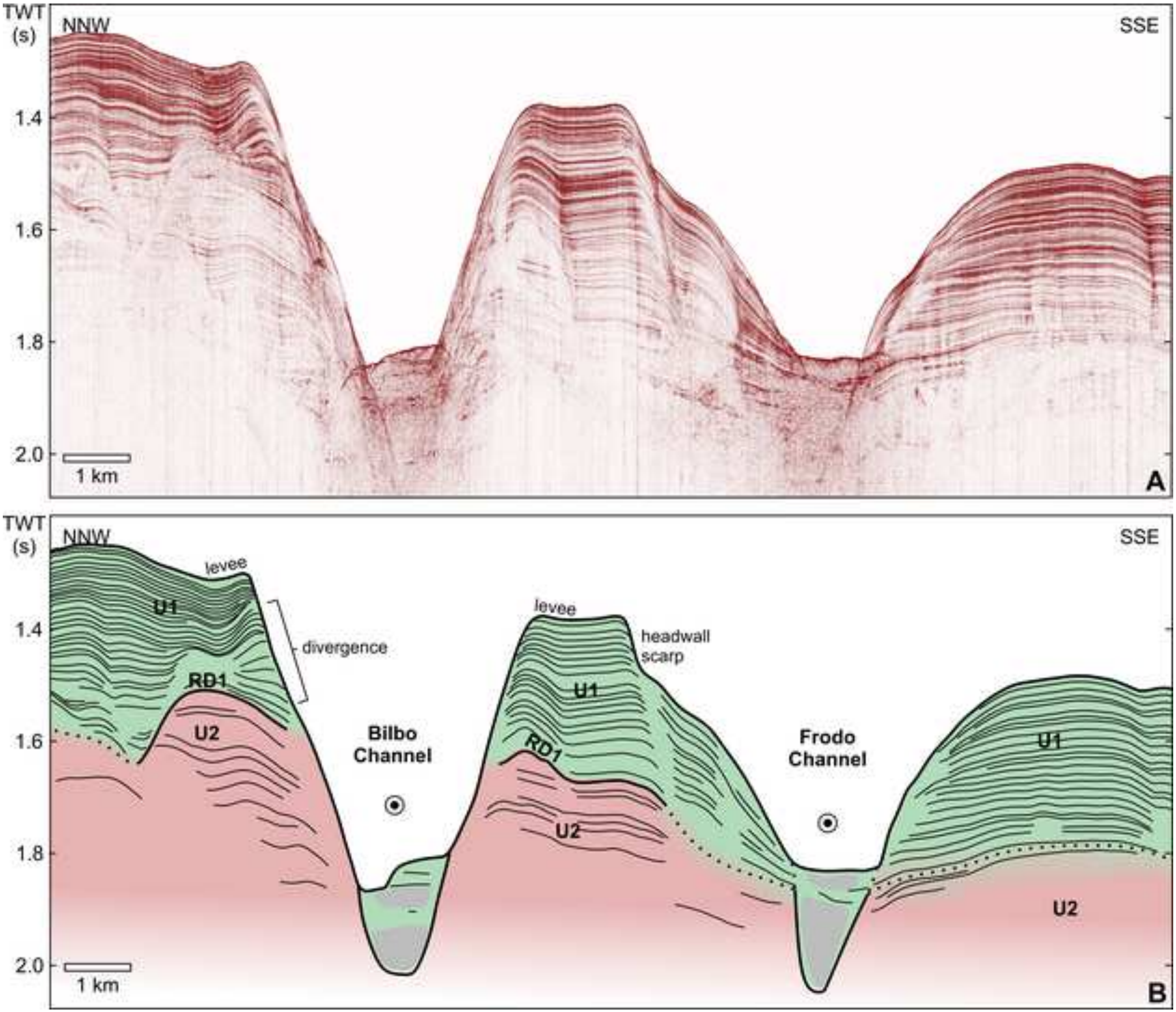

Figure8

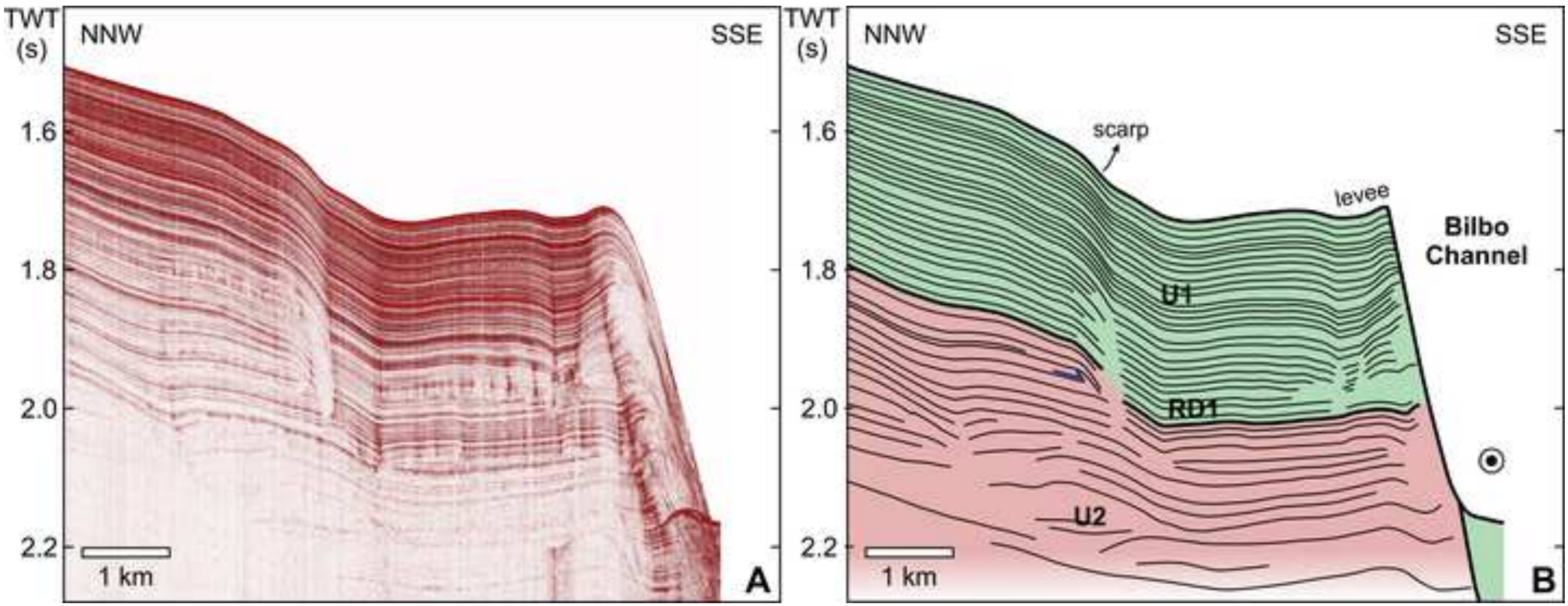
TWT (s)
NNW
SSE
1.6
1.8
2.0
2.2
1 km
A
TWT (s)
NNW
SSE
scarp
levee
Bilbo Channel
U1
RD1
U2
1.6
1.8
2.0
2.2
1 km
B

Figure9

Click here to access/download;Figure;FIG9.tif

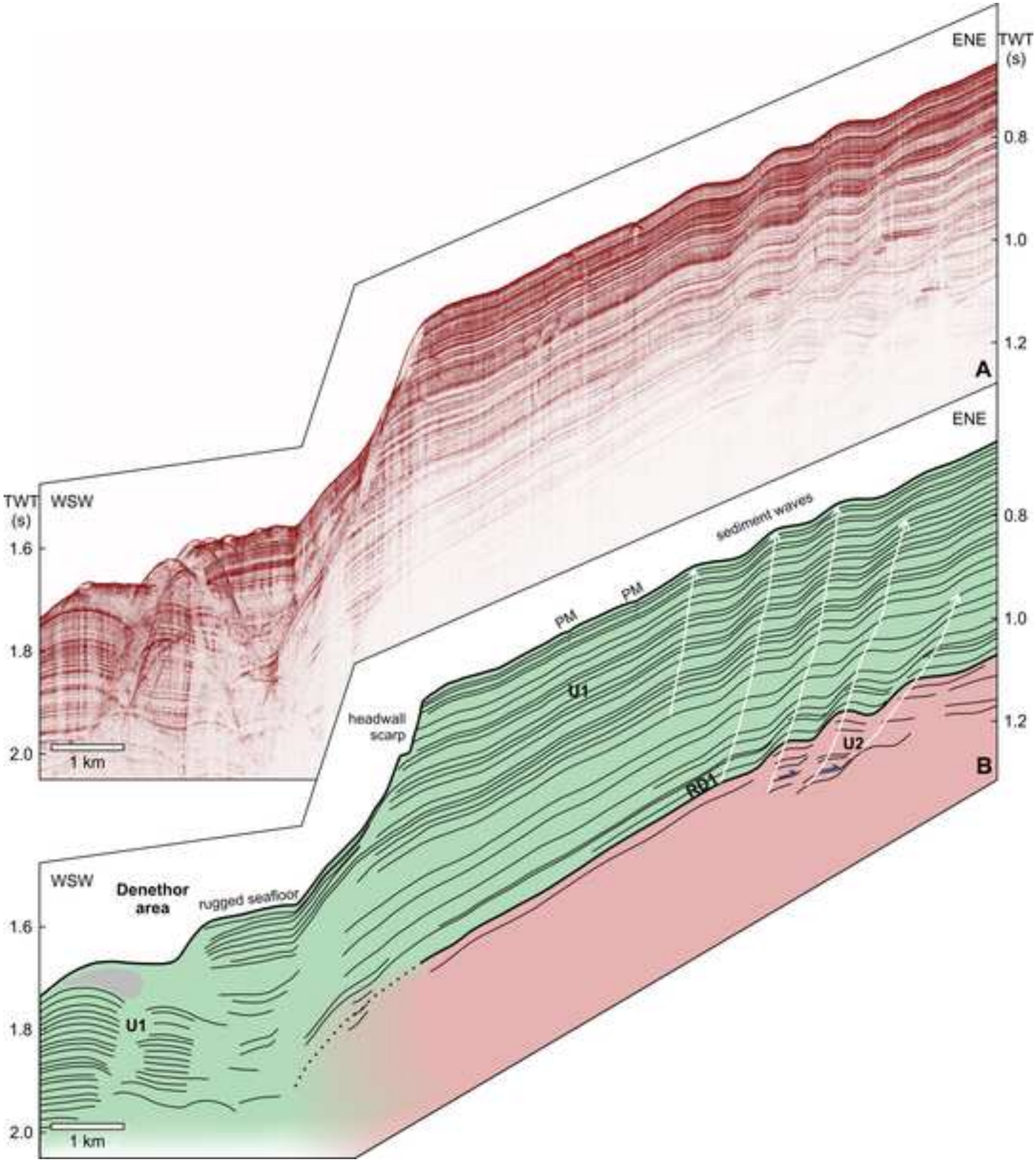

Figure10

Click here to access/download;Figure;FIG10.tif

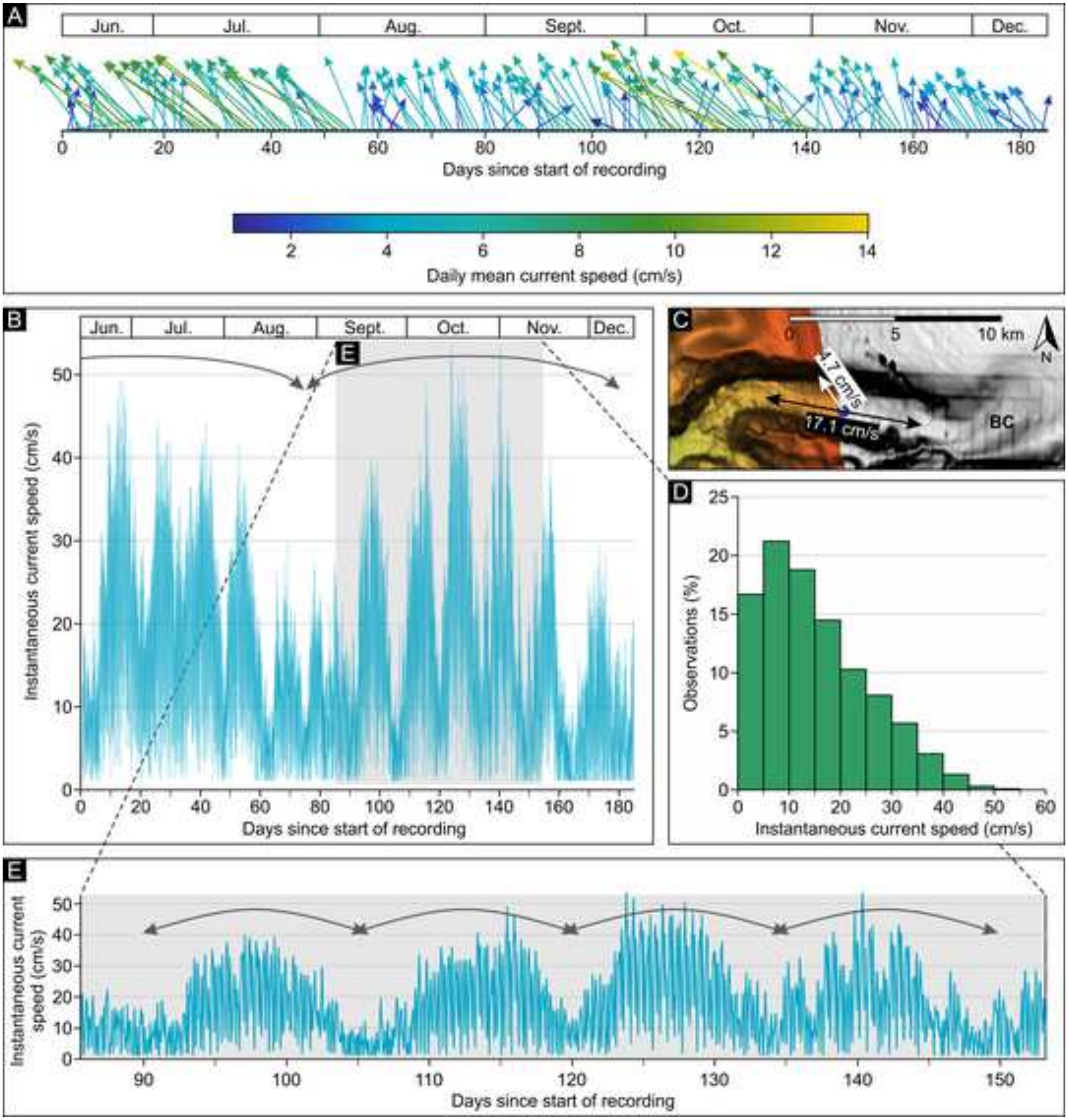

Figure11_edited

Click here to access/download;Figure;FIG11_edited.tif

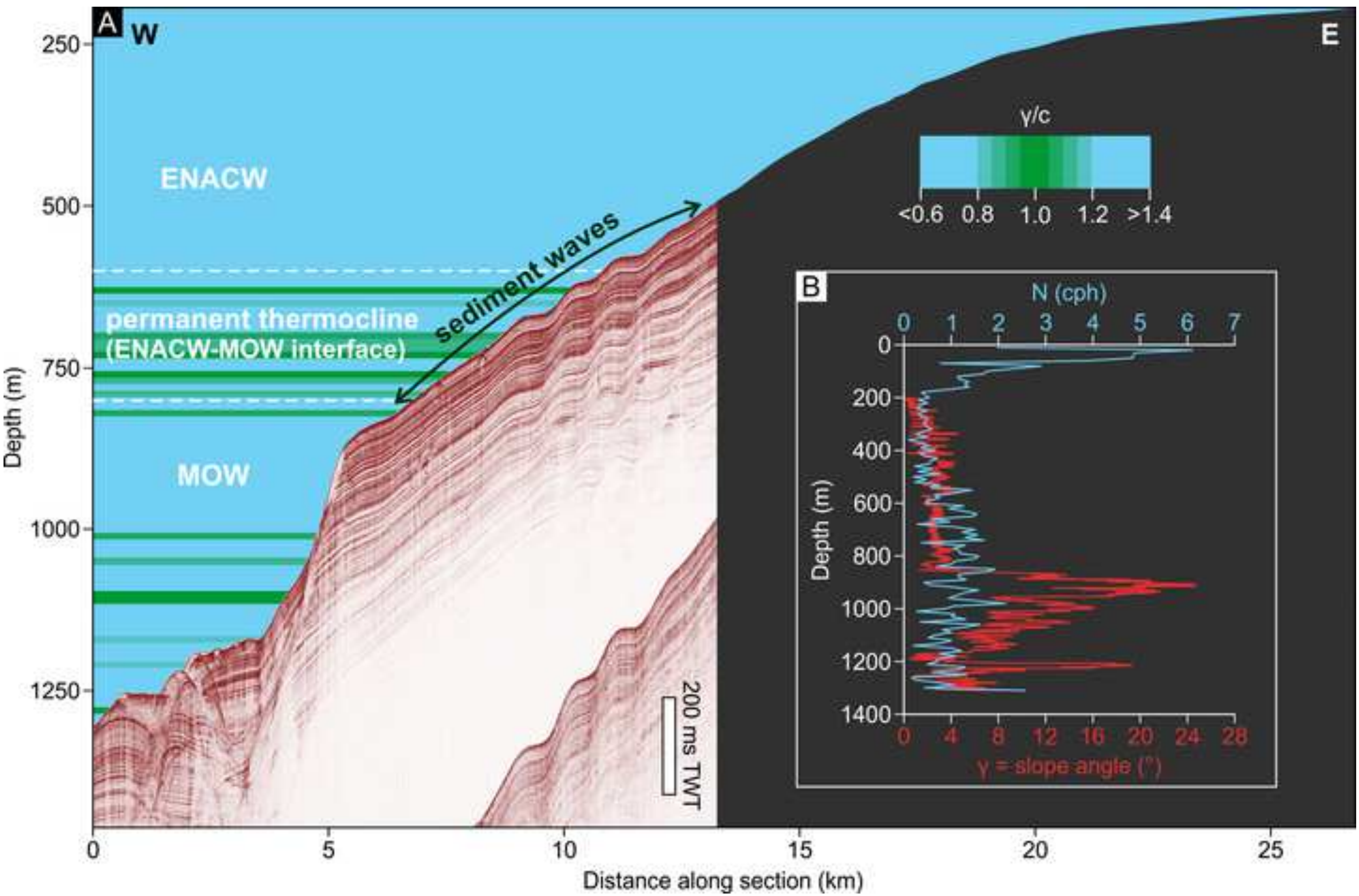

Figure1_edited

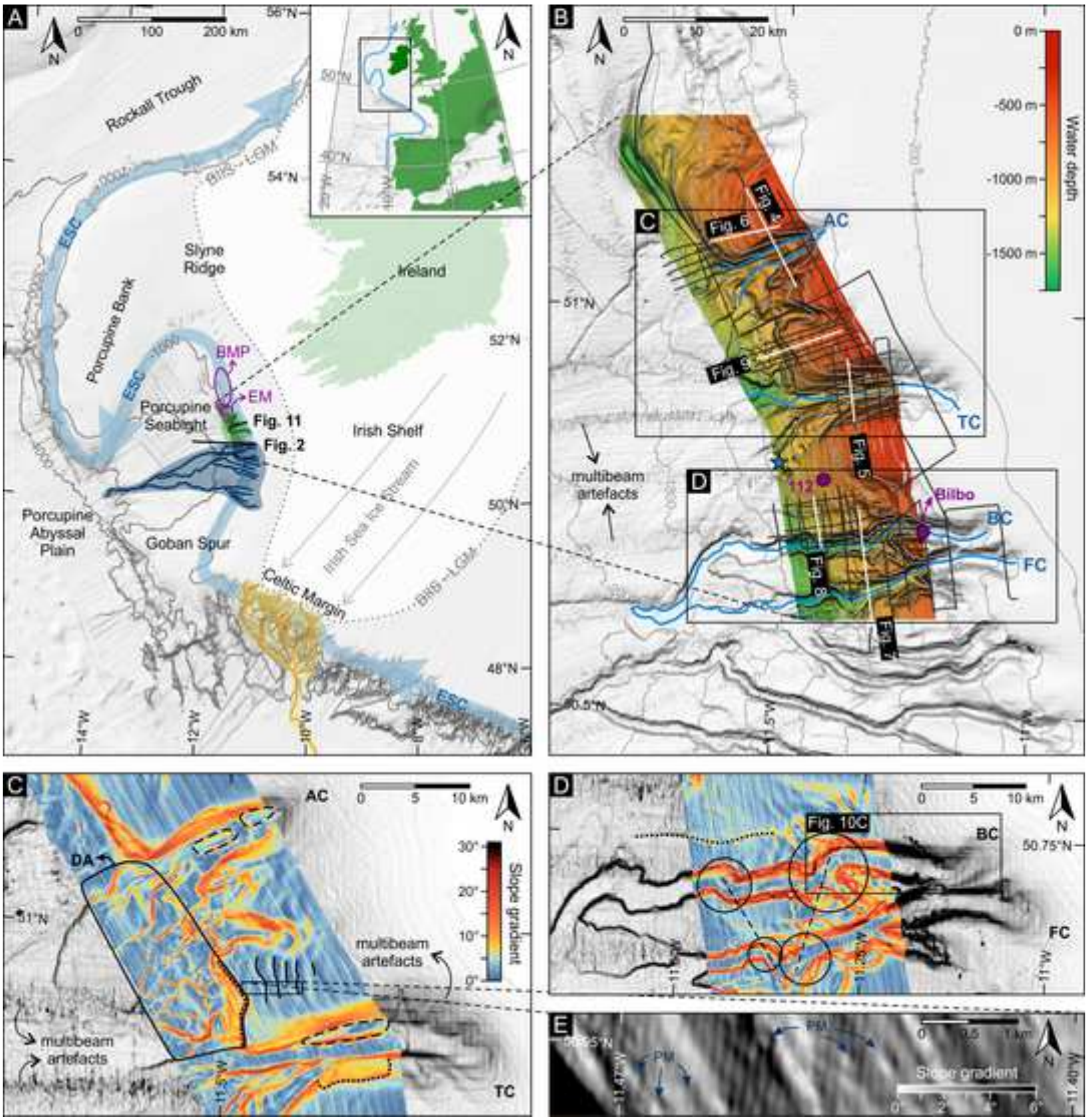

Figure4_edited

Click here to access/download;Figure;FIG4_edited.tif

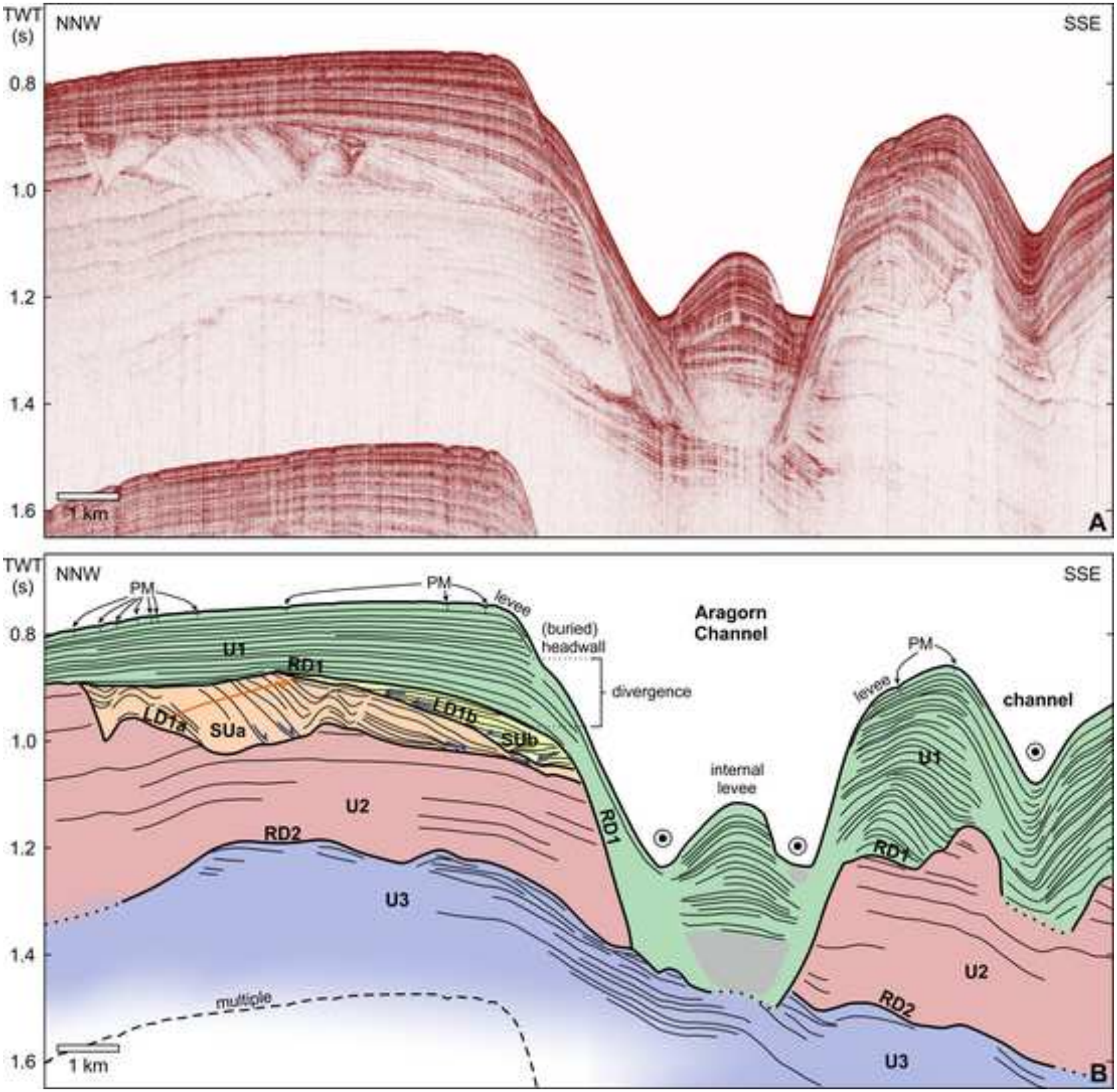

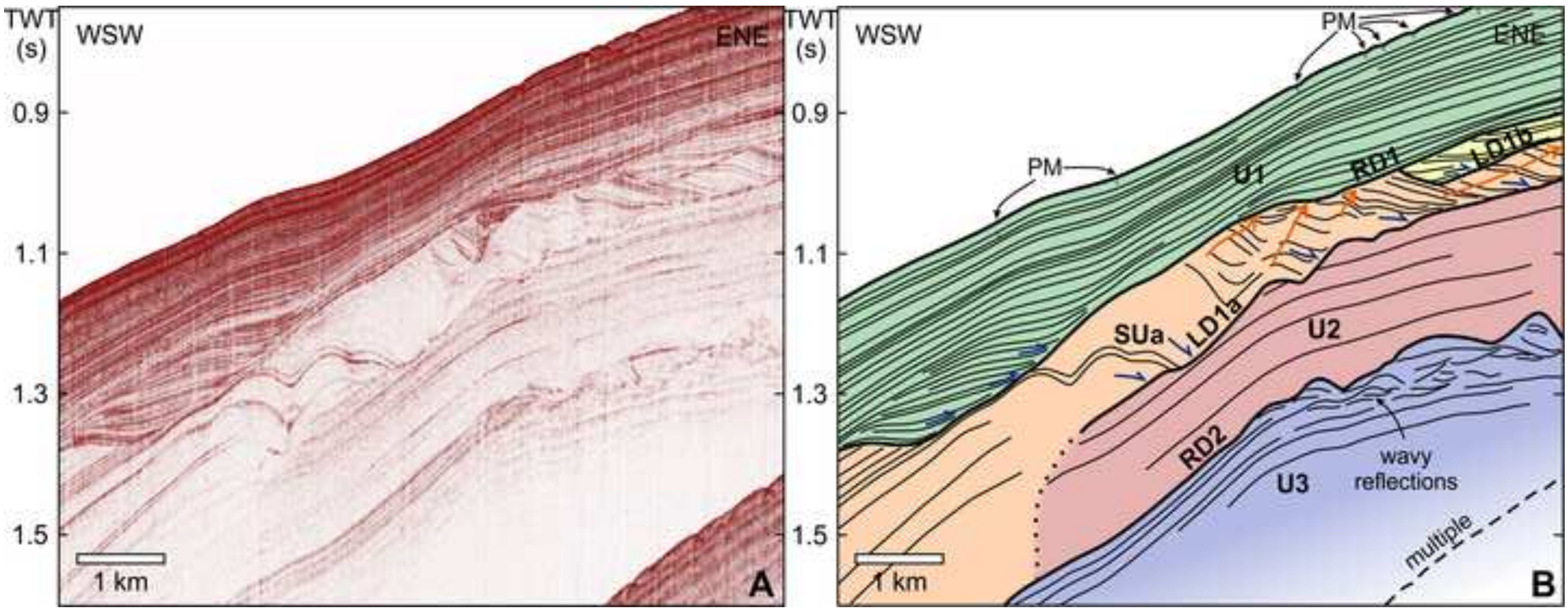
TWT (s)
WSW
ENE
0.9
1.1
1.3
1.5
1 km
A
TWT (s)
WSW
ENE
PM
PM
U1
RD1
LD1b
SUa
LD1a
U2
RD2
U3
wavy reflections
multiple
1 km
B

Table 1

	1999	2001	2003	2006	2018
Source	sparker	sparker	sparker	sparker	sparker
Energy	500 J	500 J	500 J	500 J	600 J
Sampling frequency	4 kHz	8 kHz	5 kHz	8 kHz	8 kHz
Shot interval	2.5-4 s	3 s	3 s	3 s	3 s
Vessel velocity	3-4.5 kn	2-4.1 kn	0.3-3.3 kn	3 kn	3 kn